INFORMATION TO USERS

This manuscript has been reproduced from the microfilm master. UMI films the text directly from the original or copy submitted. Thus, some thesis and dissertation copies are in typewriter face, while others may be from any type of computer printer.

The quality of this reproduction is dependent upon the quality of the copy submitted. Broken or indistinct print, colored or poor quality illustrations and photographs, print bleedthrough, substandard margins, and improper alignment can adversely affect reproduction.

In the unlikely event that the author did not send UMI a complete manuscript and there are missing pages, these will be noted. Also, if unauthorized copyright material had to be removed, a note will indicate the deletion.

Oversize materials (e.g., maps, drawings, charts) are reproduced by sectioning the original, beginning at the upper left-hand corner and continuing from left to right in equal sections with small overlaps. Each original is also photographed in one exposure and is included in reduced form at the back of the book.

Photographs included in the original manuscript have been reproduced xerographically in this copy. Higher quality 6" x 9" black and white photographic prints are available for any photographs or illustrations appearing in this copy for an additional charge. Contact UMI directly to order.

U·M·I

University Microfilms International
A Bell & Howell Information Company
300 North Zeeb Road, Ann Arbor, MI 48106-1346 USA
313/761-4700 800/521-0600

Order Number 1345425

Optical identification of a subset of IRAS SSC sources: A test of the reliability of the SSC Catalog

Clemens, Cathleen McGunigle, M.S.

The University of Arizona, 1991

U·M·I
300 N. Zeeb Rd.
Ann Arbor, MI 48106

OPTICAL IDENTIFICATION OF A SUBSET OF IRAS SSC SOURCES: A TEST OF THE RELIABILITY OF THE SSC CATALOG

by
Cathleen McGunigle Clemens

A Thesis Submitted to the Faculty of the
DEPARTMENT OF ASTRONOMY
In Partial Fulfillment of the Requirements
For the Degree of
MASTER OF SCIENCE
In the Graduate College
THE UNIVERSITY OF ARIZONA

1991

STATEMENT BY AUTHOR

This thesis has been submitted in partial fulfillment of requirements for a Master of Science at The University of Arizona and is deposited in the University Library to be made available to borrowers under rules of the Library.

Brief quotations from this thesis are allowable without special permission, provided that accurate acknowledgment of source is made. Requests for permission for extended quotation from or reproduction of this manuscript in whole or in part may be granted by the head of the Astronomy Department or the Dean of the Graduate College when in his or her judgment the proposed use of the material is in the interests of scholarship. In all other instances, however, permission must be obtained from the author.

SIGNED: Cathleen M. Clemens

APPROVAL BY THESIS DIRECTOR

This thesis has been approved on the date shown below:

Frank J. Low
F. J. Low
Professor of Astronomy

July 22, 1991
Date

ACKNOWLEDGMENT

My advisor, Frank, has the patience of a saint. Fortunately for me, he believed the virtues and responsibilities of motherhood were no less important than those of a graduate student.

Roc Cutri was, in effect, my drop-everything-now-and-explain-this advisor. He was always willing to help me with all questions concerning my data, programming and basic astronomy. Even after I moved to Boston, he was just an email message away. He wrote countless programs for my data reduction.

Kimberly Dow, namesake of my second daughter, helped me (*every* semester!) remain registered as a university student *in absentia* (no small feat at UA) and sent me countless email messages boosting my confidence. She always told me I'd finish, though I usually had my doubts. I'm happy to say you were right, Kim.

My committee members were kind enough to offer their time to read my thesis and create questions far beyond my capabilities to answer.

John Huchra, another patient soul, allowed me to spend an amount of time which will remain unmentioned on my thesis research while on the job, and even paid my way to Tucson for my defense!

Finally, I would certainly not be writing this if it were not for my husband, Dan, my advisor-in-residence. Without his gentle urging and constant support, advice, and programming expertise, this thesis would not have been written.

Thank you all.

DEDICATION

To my husband, Dan – a strong and loving motivator,

and

to my daughters, Maggie and Kimberly – such sweet distractions

TABLE OF CONTENTS

LIST OF FIGURES

LIST OF TABLES

ABSTRACT

The Infrared Astronomical Satellite (IRAS) Serendipitous Survey Catalog (SSC) was constructed from pointed observations made by the satellite when it was in Additional Observations (AO), *i.e.*, non-survey, mode. Analysis of the SSC shows that it contains a higher percentage of sources which have been detected only at 60 μm than are found in the IRAS Point Source Catalog (PSC). This could reflect the existence of a large population of faint extragalactic (galaxian) objects due to the increased sensitivity of the SSC relative to the PSC, especially in the 60 μm band, or simply be a result of spurious sources in the SSC. Inspection of cirrus contamination over each AO showed that it had little or no effect on the high 60 μm-only source count. An automated optical identification program presented here indicated that 60 μm-only sources were as likely to have optical counterparts as all other sources, and more likely than randomly-placed artificial sources. The SSC sources studied had, on average, one more optical source found nearby than did artificial data: probably the optical counterpart to the IRAS source. These results support the validity of the 60 μm-only sources and the SSC in general.

I. INTRODUCTION

A. IRAS and the IRAS SSC

The Infrared Astronomical Satellite (IRAS) Serendipitous Survey Catalog (SSC) (Kleinmann *et al.* 1986, hereafter KCYLG) was produced using data gathered during the Pointed or Additional Observation (AO) program. During these non-survey observations, fields ranging in size from 0.5° x 0.6° to 0.5° x 6.0° were scanned at one-half the angular rate of that for the survey mode, with the field centered on some particular target position. A total of 1813 AO fields cover 1108 deg^2 on the sky (see Figure 1). Analysis of these data led to the SSC containing 43,886 point sources found in these fields, of which 29,420 sources are at galactic latitudes $|b^{II}| \geq 30°$. More than 27,000 sources had not been previously cataloged. The 90% completeness limits derived from the observed differential Log N *vs.* Log F curves are 120, 150, 120, and 440 mJy at 12, 25, 60, and 100 μm, respectively (KCYLG). These values are considerably more sensitive (*i.e.*, lower) than those for the IRAS Point Source Catalog (PSC): the PSC equivalent values are 400, 500, 600 and 1000 (IRAS Explanatory Supplement 1988).

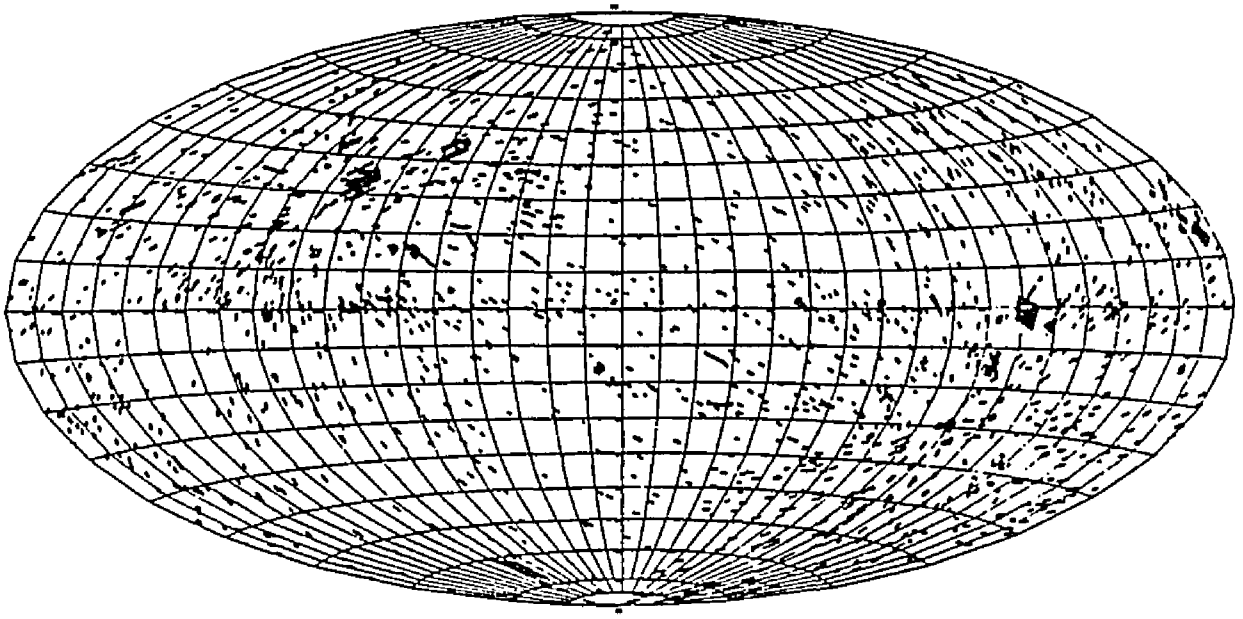

Figure 1. Distribution of AO Fields on the Sky in Galactic Coordinates. Each rectangle corresponds to one AO, characterized by a central coordinate, length and orientation angle defined as East of North on the sky.

B. The Reliability of the IRAS SSC

Spectral analysis of the sources contained in the SSC shows that it contains a much larger percentage of sources which have been detected only at 60 μm (24.6%) than is contained in the PSC (7.8%) (KCYLG). To properly interpret these results, one must ascertain that the surplus 60 μm-only sources are not spurious artifacts of the source extraction technique but are indeed *bona fide* astronomical point sources.

Several known types of objects would have peak IRAS emission at 60 μm. Galaxies typically have 60 μm-dominated IRAS fluxes, especially starburst galaxies (Huchra 1987); galactic objects with 60 μm fluxes dominating are most often highly evolved stars (Rowan-Robinson *et al.* 1984). Clumps in cirrus could appear to be point sources and be detected only at 60 μm. A surplus of 60 μm-only sources may be an indication of either a new population of objects which have peak IRAS emission at 60 μm or more of a known population with similar characteristics. The extra SSC 60 μm-only sources could simply be faint enough to have been missed by the PSC, but just above the detection limits of the SSC due to its increased sensitivity especially at 60 μm. However, the surplus 60 μm-only sources could be largely due to spurious detections by the satellite and be counterindicative of the

density of such objects on the sky.

Independent of their astronomical nature, the *overabundance* of 60 μm-only sources found in the SSC is in part due to the increased sensitivity of the four IRAS bands in the SSC relative to the PSC. Figure 2 shows the 90% completeness flux limit curves for a) the PSC, b) the SSC and c) an adjusted SSC. The adjusted SSC curve was made by increasing the 60 μm band limit to 0.18 Jy and the 100 μm limit to 0.30 Jy so that the curve imitated that of the PSC (having the same colors). After this adjustment, the percentage of 60 μm-only sources in the SSC dropped from 25 to 5%, becoming much more like the PSC (8%). The adjusted SSC is dominated by 12 and 25 μm emission objects, as is the PSC.

To determine whether the 60 μm-only sources are reliable or spurious, a program was initiated to detect them independently. Cutri *et al.* (1987) showed that IRAS sources which were detected in more than one band were highly reliable. Since the sources of interest were only detected in the 60 μm band, we tried to identify optical counterparts to the SSC sources in the blue band, using a statistically significant number of the SSC sources. The cirrus contamination over each field was also studied to see if cirrus were a major contributor to the excess 60 μm detections.

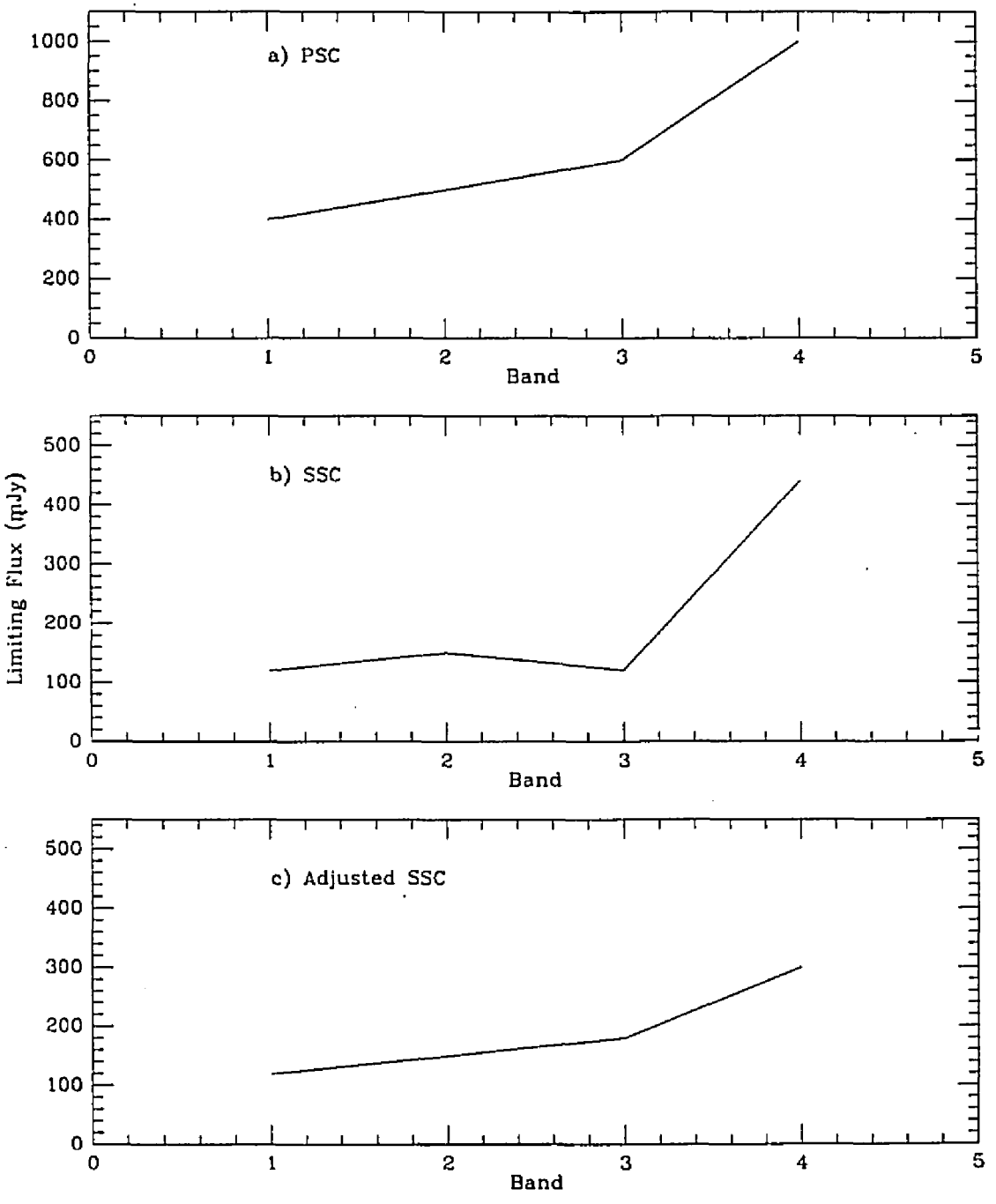

Figure 2. The 90% completeness limits in the four bands measured by IRAS for a) the PSC, b) the SSC and c) the adjusted SSC. The 60 μm band in the SSC is much more sensitive relative to the other IRAS bands. Adjustment of the 60 and 100 μm bands so that the limiting fluxes are 0.18 and 0.30 Jy makes the SSC colors the same as the PSC ones.

C. Optical Identification of a Subset of IRAS SSC Sources

Detection and classification of the optical counterparts for a sub-sample of SSC sources could help indicate whether the SSC sources are real or spurious, and if real, could crudely indicate the nature of the sources. For example, if the 60 μm-only SSC sources are always optically associated with faint spiral galaxies with a correlation probability exceeding that of randomly selected sky positions, one could believe that the SSC 60 μm-only detections were reliable. If many or most of the 60 μm-only sources are not found to be associated with an optical counterpart, and the cirrus contamination over the AO fields is low, then these SSC sources would be considered to have a high probability of being spurious detections. If the cirrus contamination were high, the sources would appear to be knots in the cirrus instead of true point sources.

The sources from 53 AOs with $|b^{II}| \geq 30°$ were studied here by two independent methods. An automated method involved digitization of photographic plates, while a manual method employed a systematic visual examination of photographs of the same fields.

D. Introduction to the Remainder of the Thesis

In Chapter II, selection of the subset of the SSC and collection and reduction of the data from the automated optical identification program are discussed. The characteristics of this sample are presented and compared to those of the SSC in general. The photometric conversion from the digitization process to a standard photometric system is described. The manual optical identification results are tabulated and summarized in this chapter. Cirrus contamination over each AO field is discussed.

In Chapter III, a method for a probabilistic identification of the optical counterparts of the IRAS SSC sources found in the automated search is presented in detail. The method used to estimate the association probability for each of the typically 2 to 5 optical sources found within each IRAS SSC positional error box is based on two criteria. The first is a two dimensional spatial offset probability, computed from the gaussian positional errors of bright stars and galaxies detected by the SSC (KCYLG). The second probability reflects the Poisson nature of the distribution of the optical source counts in various magnitude bins. This second probability is related to the likelihood of association with a source of a particular magnitude, given the distribution of such sources across the larger AO field. The

optical counterparts found around the positions of SSC sources are compared to those of random positions on the sky: artificial data.

In Chapter IV, the characteristics of the optical sources most likely associated with the SSC sources are examined. (B−60) colors of the 60 μm-only sources are compared to those of galaxies from the PSC, and quasars and evolved stars in the SSC.

Chapter V summarizes the findings and assesses the SSC reliability, as probed by this optical investigation of the 60 μm-only sources.

II. DATA

A. Spectral Characteristics of IRAS SSC Sources

Spectral analysis of all IRAS SSC sources shows that the SSC contains a much higher percentage of sources detected only at 60 μm than does the IRAS PSC (KCYLG). Figure 3 contains a histogram of spectral information from a) the complete PSC, b) the complete SSC, c) the SSC subset chosen for this study (see section B below) and d) an adjusted SSC. The bins contain the detection possibilities in the four bands observed by IRAS. A detection in a certain band is denoted by a one, while a zero denotes a non-detection. For example, 1000 refers to a source which was detected only at 12 μm; 0011 refers to a source detected at 60 and 100 μm only. No information about the quality (*i.e.*, the signal-to-noise ratio) of the detection is used here; any detection in a band is denoted by a one (IRAS Explanatory Supplement 1988). These histograms show that the bin labeled 0010 (sources detected only at 60 μm) contains a much higher percentage of sources in the SSC than it does in the PSC (compare Figures 3a and b). The SSC subset was chosen to have an even higher percentage of these sources (Figure 3c). However, when the

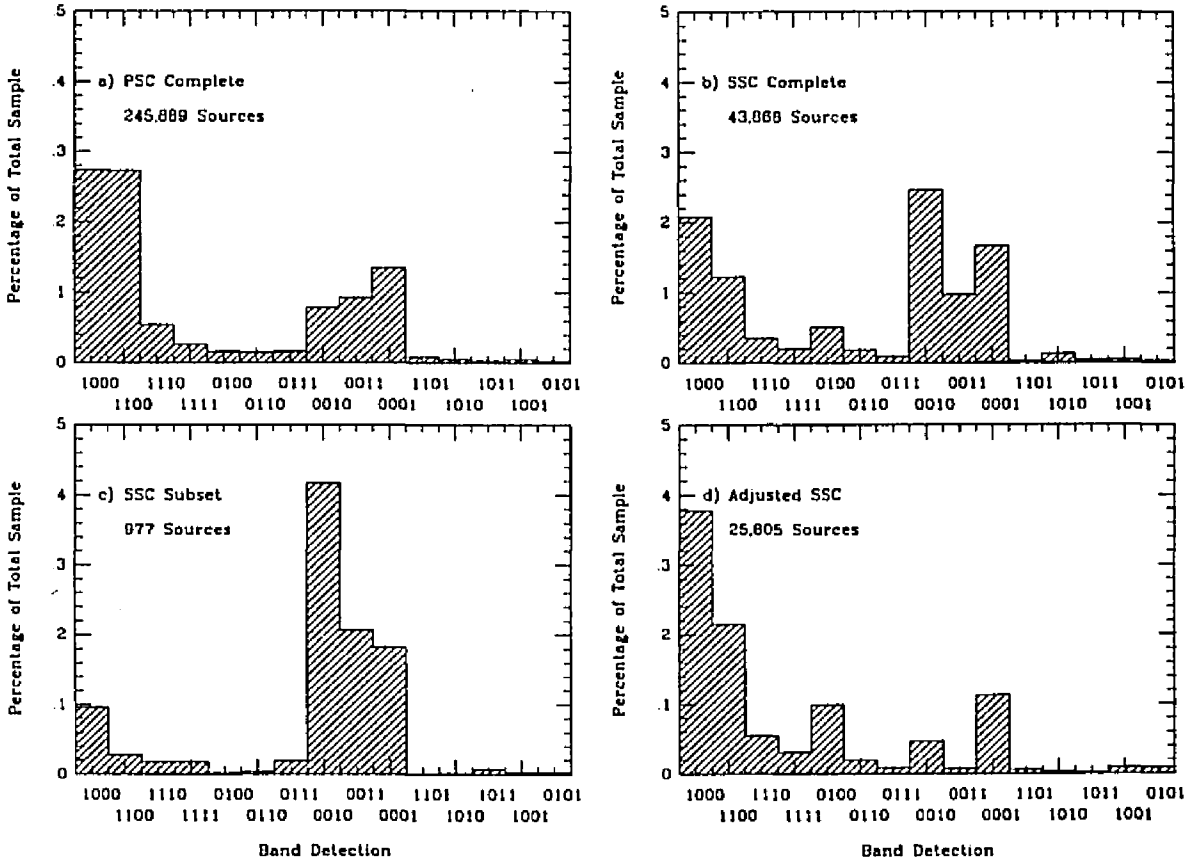

Figure 3. Percentage of the total number of sources in each sample *vs.* band detection bins for a) the complete PSC, b) the complete SSC, c) the SSC subset chosen for this study, and d) the adjusted SSC, whose limiting 60 and 100 μm fluxes are 0.18 and 0.30 Jy. The band detection bins are as follows: 1000 indicates that a source was detected at 12 microns only; 1100 indicates detection at 12 and 25 microns only, etc. Note that the SSC complete sample contains many more sources in the bin 0010 than does the PSC. However, when the 60 and 100 μm flux limits are raised, the histogram appears more like that of the PSC.

60 μm sensitivity limit is adjusted to 0.18 Jy and the 100 μm limit becomes 0.30 Jy, the histogram in Figure 3d resembles more closely that of the PSC.

B. Selection of Comparison Fields

The SSC utilities (R. Cutri, priv. comm.) are a set of programs which allow the user to select SSC data by various parameters and tabulate statistics about the chosen sample. The SSC utilities were used to select 68 AO fields which contain the highest densities of 60 μm detections at latitudes $|b^{II}| \geq 30°$ for this study. High latitude AO fields were chosen in order to avoid confusion within the galactic plane. Magellanic cloud AOs were excluded, as were AO fields containing other very nearby galaxies since they could potentially skew the results. These very nearby galaxies are bright and therefore are very likely real sources. In the sample chosen, we tried to include 60 μm sources over a large range of fluxes so that identification of them supported the existence of all 60 μm sources as real. The AO fields with the highest densities of 60 μm detections were chosen to minimize optical plate scanning time and yet obtain a statistically large sample of comparison sources. The high density fields were also selected because they represent the most anomalous cases. Over 1200 total sources were in the initial selection. The National Optical Astronomy

Observatory (NOAO) PDS was used to scan the regions of the sky covered by the AO fields on the Palomar Observatory Sky Survey (POSS) and European Southern Observatory (ESO) blue (O) plates. The blue plates were scanned because they are about one magnitude deeper than the red (E) plates and because blue magnitudes are traditionally studied and are more readily available.

The sample of SSC sources used for this study includes *all* sources in those AO fields which contain the highest densities of 60 μm detections. Consequently, the sample contains a large percentage of 60 μm-only sources (Figure 3b) but also includes sources with other band detection characteristics.

Some AO fields were rejected because they were found to contain bright, saturated objects on the sky survey plates which could not be scanned with the PDS. The sample chosen for PDS scanning contained 960 sources in 53 AO fields, of which 403 were 60 μm-only sources. There were 9 repeat sources: sources which appeared in two overlapping AO fields; four of the nine were 60 μm-only sources. One set of the repeats was deleted from the sample. The final sample of fields successfully scanned by the PDS included 53 AO fields containing 927 SSC sources of which 389 are 60 μm-only sources; 24 of the 960 SSC sources were not within the scan areas of

the PDS. Of these 927 sources scanned, 101 are also in the PSC. The effective area of sky covered by the 53 fields is 27.7 deg^2, or 2.5% of the effective area covered by the entire SSC (KCYLG). Figure 4 shows the differential Log N - Log F histograms of the four bands for this subset. The number of detections is indicated in each band in each plot.

C. POSS/PDS Scanning Method

The NOAO PDS is a measuring engine to which a CCD camera has been mounted (Monet 1983). It is used for astrometry and photometry of objects on photographic plates. It has 480 x 480 rectangular pixels which scale to a field of view of 6400 x 5200 microns in the x and y coordinates, respectively. These dimensions correspond to an image size of about 7 x 6 arcmin on POSS plates. Single images may be collected for areas smaller than the field of view of the detector, or multiple images may be combined as the detector scans over larger areas. A photographic plate is set on the PDS $x-y$ translation stage at any arbitrary angle and is stepped (under computer control) across the field of view of the fixed CCD in a raster pattern. The scan area is uniformly illuminated from the underside of the plate using an adjustable brightness light source so that the background emission level

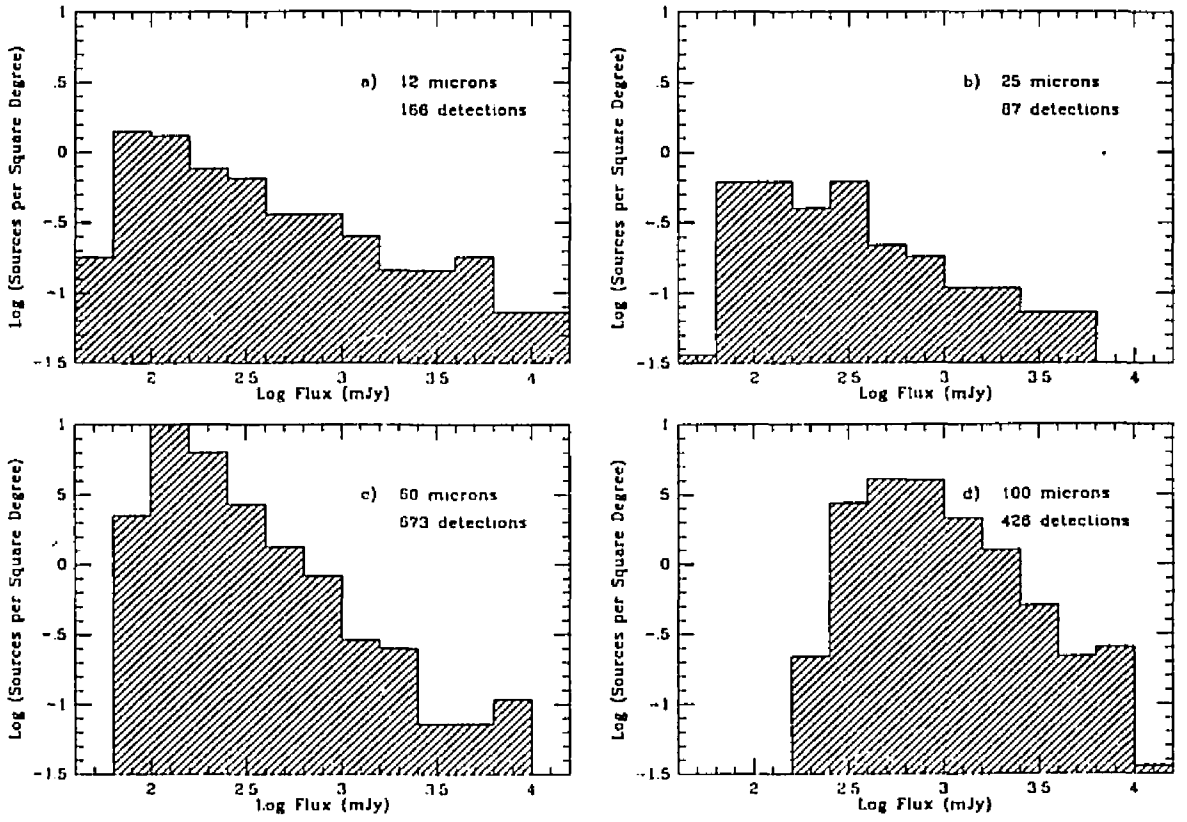

Figure 4. Differential Log N - Log F curves for the four band detections of the 960 SSC sources in the subset studied in this work. The number of detections in each band is indicated in each plot. No flux limits have been imposed here.

for each plate can be normalized; this is especially important when the instrumental magnitudes from multiple plates are to be compared to a standard photometric system. The dynamic range of the detector is 256 digitizing units (d.u.). Software and much of the hardware interface were developed by Monet (1983) and reduction software was extended from Monet's software by R. Wade (priv. comm).

Tabulated in the PDS output are the following parameters for each object detected by the source detection software's processing of the CCD data: displacement coordinates, x and y, in machine units; an instrumental (PDS) magnitude; a measure of elongation of the object, E; the size of the object measured in CCD pixels, S; a measure of the brightness of the sky averaged over the pixels surrounding each object, measured in d.u.; and a saturation flag which indicated if an object was too dark (*i.e.*, bright on the sky) to be photometered. The size of the object is determined by the image radius, a mean radius assuming circular annuli based on the growth curve of the image intensity.

At the beginning of each scanning session, the PDS illumination level was adjusted so that the background light level averaged about 80 d.u. in blank-sky regions of the plate. This was particularly important because not only were many

POSS plates used, but ESO plates, which have much darker (*i.e.*, brighter) background levels (denser fog level), were used for the southern declination fields. This adjustment helped to reduce the variation of the photometric zero point between plates. The grain of the photographic emulsion caused a standard deviation of the background emission of less than 8 d.u. over the area of each field.

For each field, five to seven SAO stars were measured and their PDS coordinates were noted. This measurement was done by manually moving the PDS stage and centering each star on cross hairs drawn on the PDS video monitor. Without repositioning the plate or resetting the machine coordinates, the AO field was then scanned. The coordinates of the SAO stars and PDS positions of those stars were presented to the NOAO programs FINDER and ASTRO to calibrate the conversion to right ascension and declination from PDS x-y coordinates. The PDS output data files thereby contained astrometry of each optical source, precise to typically less than an arcsec and always better than 2.5 arcsec. Software to convert tabulated PDS output to its final form for data analysis was written by R. Cutri (priv. comm.).

Independently measured coordinates for some of the objects around SSC sources agreed with those obtained above to within 6 arcsec, for similar astrometric preci-

sion. (See Section E 2 below)

D. PDS-to-B Magnitude Conversion

In order to use PDS scanning of POSS plates to obtain accurate photometry on a standard photometric system, a conversion must be found between the magnitudes reported by the PDS and magnitudes on a particular photometric system. U, B, V, R and I band CCD data of seven stellar (cluster) fields were obtained by L. Davis (priv. comm.; extension of Christian *et al.* 1985). The NOAO PDS was used to scan POSS plates containing these photometric standard star cluster fields. The resulting data were examined to look for a correlation between CCD-obtained B and R magnitudes and PDS-obtained blue (O) and red (E) magnitudes. Although CCD detectors have linear responses, as does the (CCD) detector on the PDS (Monet 1983), the POSS plates are photographic. Photographic response introduces nonlinearities, hence the range of magnitudes was limited and the photometric zero point of each plate varied slightly. Also, the magnitudes reported by the PDS do not scale linearly to the CCD magnitudes of the same objects.

1. Selection of Calibration Fields

Four of the seven standard fields observed by Davis were deemed suitable as

PDS fields: each is less than 6 arcmin in extent, the size of the PDS detector field of view on POSS plates. Each field has at least 15 stars spanning the magnitude range 13 to 22 in B; and each field is not overly crowded so that identification of each standard star was simple and photometry was not compromised by star confusion. All four of the fields are in the northern hemisphere. For each CCD field, both the POSS blue (O) and red (E) plates were scanned by the PDS. The red plates were scanned so that a future color correction could be applied to the SSC PDS data. However, no color corrections are included in the data presented in this thesis. Astrometry of the stars in each field was performed using the ASTRO program and positions of the individual stars were obtained to an uncertainty of one arcsec or less.

2. Calibration

Derived stellar data for the four photometric standard fields were plotted as PDS *vs.* CCD magnitude for each color and are presented in Figure 5. It is evident from Figure 5 that a systematic error is introduced when data from different plates (*i.e.*, fields), are combined. Two third-order polynomials were fitted separately to

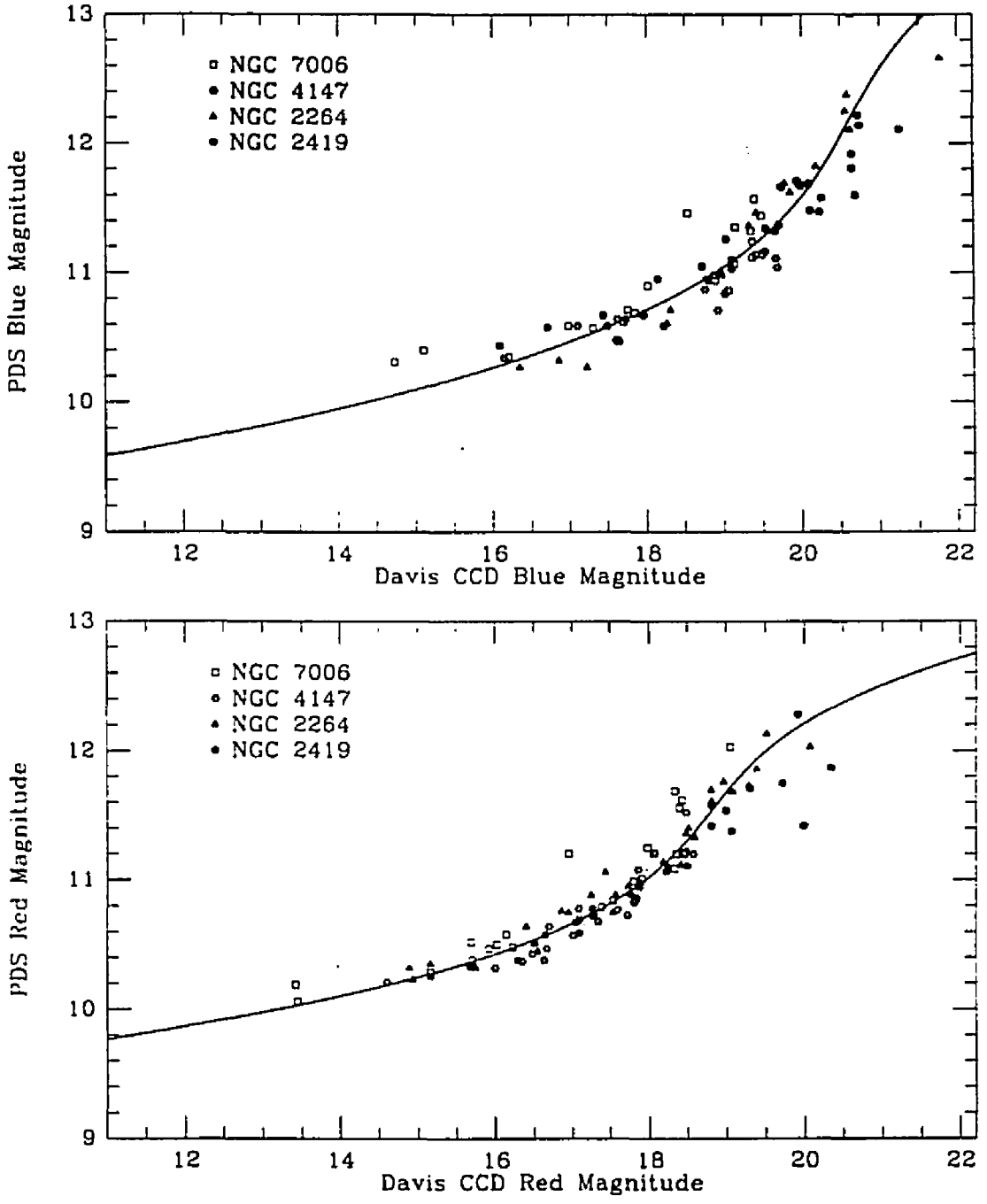

Figure 5. Calibration curves for PDS to CCD magnitude conversion for four red and blue standard fields from separate POSS plates. The separate symbols indicated by the legend show each star cluster plotted and the best fit curve to the data. Calibration curve parameters are given in Table 1.

the blue and red data; the equation used to represent the data is

$$CCD = A_1 + A_2PDS + A_3PDS^2 + A_4PDS^3 \quad (1)$$

where CCD and PDS refer to those magnitudes. Table 1 contains the best fit parameters: constants, uncertainties and magnitude ranges over which this fit is reliable. The magnitude conversion uncertainty, σ, pertinent to this study is the one for all four fields of blue data: 0.5 CCD mag.

In an attempt to identify the source of the systematic error in PDS magnitudes from different plates, many plots were made of the PDS parameters. The mean sky value for each star cluster field and color was calculated from the PDS sky values around each source in each field. Magnitude residuals (which are the differences between the object magnitudes and the fit magnitudes) were calculated for each object from the fits in Table 1. For each field and color, plots were made of the magnitude residuals of each source *vs.* the following: sky residuals (which are differences between the mean sky value of a field and the sky value for each object), sky value, magnitude, image size of each object measured in PDS pixels, the log of the sky value, the log of the number of pixels, and the log of the sky residual. No obvious trends were seen in the plots to implicate any single parameter as being

Table 1

CCD-PDS CROSS-CALIBRATION PARAMETERS

	Four NGC Fields		NGC2264 Only	
Constants	Blue	Red	Blue	Red
A_1	−752.10	−1525.8	−441.18	−1021.2
A_2	188.72	399.11	111.92	264.53
A_3	−15.436	−34.487	−9.1288	−22.556
A_4	0.42286	0.99660	0.25059	0.64492
σ_{CCD} (mag)	0.500	0.407	0.350	0.278
Data Points Used	82	96	19	28
Approx. Valid Ranges (mag):				
CCD	13-21.5	12-20	13-21.5	12-20
PDS	9.8-13.0	9.9-12.2	9.5-13.0	9.8-12.2

responsible for the systematic error; *e.g.*, magnitude residuals did not increase as a function of magnitude. Only the photometric zero point, as measured by the mean sky value for each field, varied from plate to plate. It appears that each plate would have to be independently calibrated to remove the systematic error. Since no such calibration was produced for these plates, the systematic error remains in all data reported here.

Another calibration curve was obtained using the data from one plate only. NGC2264 data were plotted and fitted as before. Here, uncertainties of 0.35 CCD mag for the blue and 0.28 CCD mag for the red were obtained (see Figure 6). Polynomials of the form of Equation 1 were fitted and coefficients for the fits are also listed in Table 1. Similar, lower uncertainty curves could be used for converting PDS measurements from a single plate provided similar calibration data existed.

E. Other Data Analysis

1. Additional PDS Parameters

A separate sample of 103 objects of known identity (*i.e.*, 52 stars and 51 galaxies) was used to identify a correlation between the PDS parameters which measure object elongation, E (dimensionless), size, S (measured in pixels), and the PDS

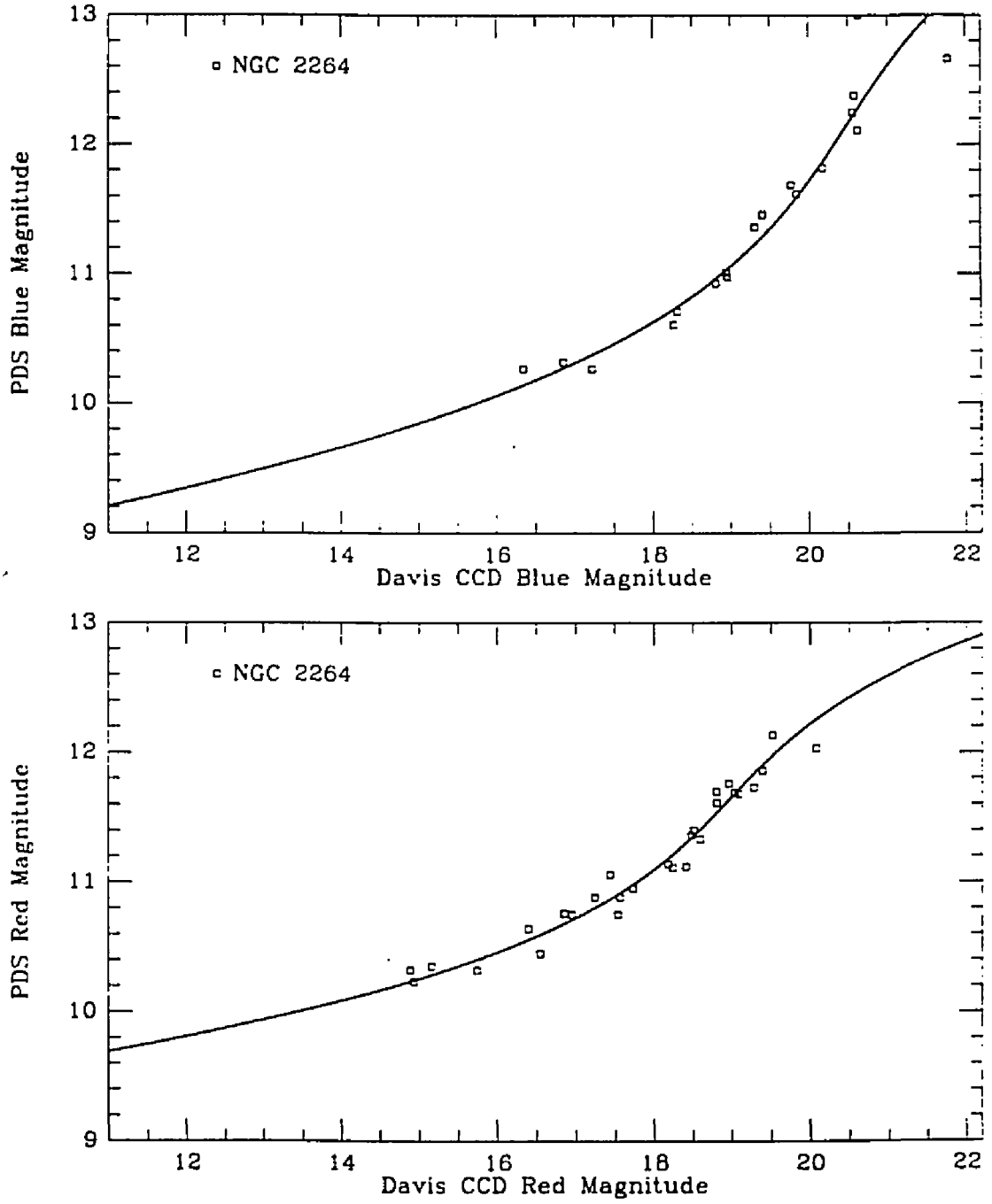

Figure 6. Calibration curves for PDS to CCD magnitude conversion for NGC2264 cluster data from a single POSS plate for each color. Note that the scatter in the fit in Figure 5 is greatly reduced here by using data from one plate. The calibration curve parameters are given in Table 1.

magnitude. This sample was derived from the previously discussed photometric standard star cluster data and the Harvard-Smithsonian Center for Astrophysics (CfA) Redshift Survey (Huchra *et al.* 1991). *These data are independent of the IRAS SSC.* Most of the objects in this sample have PDS sizes smaller than 20 pixels. For each of these 103 identified objects, a flux was derived from the PDS magnitude using

$$\mathrm{F} = 10^{(PDS\ mag-9)}. \tag{2}$$

where the PDS mag has been scaled so that the numbers are manageable. F was divided by S^2, the area of the object, to form a surface brightness, SB, using

$$SB = Log_{10}\frac{F}{S^2} \tag{3}$$

SB *vs.* E is plotted in Figure 7. The plot shows the 52 stars plotted as open squares and the 51 galaxies as filled squares. Four zones were defined. Zone g is the region where galaxies seem to dominate: the elongation of the objects is high (above 3.8) and the surface brightness is low (below 1.5). Zone s is a region where stars seem to dominate: low elongation (below 3.8) and high surface brightness (above (1.5); Zone a, where both elongation and surface brightness are low, is occupied by both stars and galaxies, as is Zone x, defined as the remaining area of the graph. These

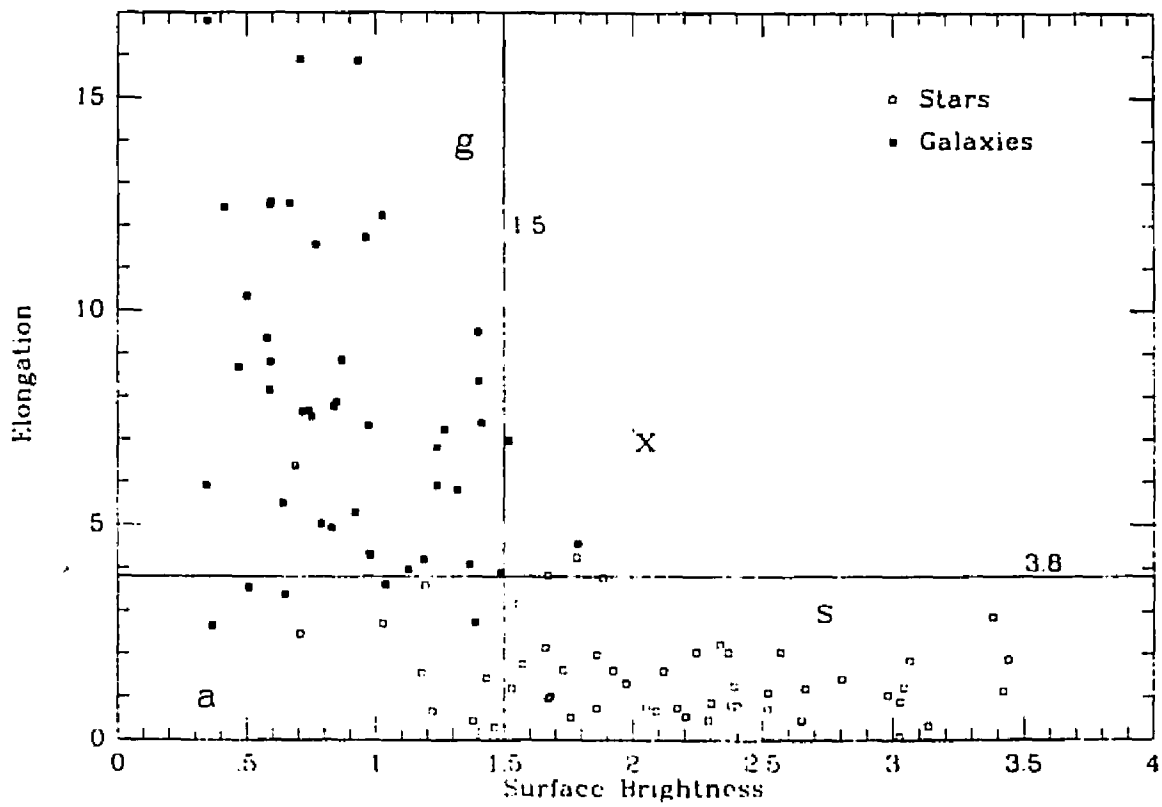

Figure 7. PDS Elongation *vs.* Surface Brightness for 103 objects of known identity. Stars are plotted in open squares and galaxies are filled squares. Four zones which are labeled are defined by the 3 σ boundaries of the separate best fits to stars and galaxies.

zones are areas where unidentified objects appear. There are 10 stars and 7 galaxies in Zones a and x. The star and galaxy data were fitted separately to straight lines. The zones are defined by the boundaries of the 3 σ fits and are labeled on the plot.

Of the 103 objects plotted, 17 appear in Zones a and x; 86 were correctly zoned. Although the brightest star plotted here is 13.5 mag, a star may be interpreted as an extended object if it were bright enough to have diffraction spikes (*e.g.*, SAO stars) or if there were 2 stars in close proximity which the PDS saw as one object; in either case, such stars would not appear round. In the proper orientation to our view, a galaxy may indeed appear round. It should not, however, have as high a surface brightness as a star, except if it were a quasar. Also, proper focussing of the PDS lenses and clean photographic plates are important to increase the incidence of correct identifications. The faintest stars detected are more likely classified as a, unidentifiable, since the surface brightness diminishes while they may still appear round.

The classifications defined here were imposed upon the optical counterpart candidates found within the error boxes of the SSC sources.

2. Manual Examination of POSS/ESO Plates for each AO

In addition to the automated PDS scanning and classification method described above, visual inspection of photographic slides of the blue POSS plates containing the AO fields was employed in an attempt to optically identify all of the chosen subsample of SSC sources as being stellar or galaxian. The slides were obtained from a uniform photographic setup. Each SSC source which showed a clearly identifiable optical counterpart had that counterpart classified as galaxian or stellar. Specifically, if an object had diffraction spikes, it was classified as stellar, and a clearly fuzzy or extended object was classified as galaxian. Not only does this information serve as a means of identifying the optical counterparts to SSC sources, it also provides a check on the automatic technique which assigns probabilities of association to each of the optical counterpart candidates found in the vicinity of each SSC source. Additionally, the reliability of the PDS software classification of candidates as galaxian or stellar could be assessed. In most of the manually examined cases (60%), the POSS slides contained optical objects near SSC sources which were too faint to classify. Five AO fields did not have available slide data. These fields were analyzed separately with the CfA Measuring Engine. These CfA data not only complete the visual inspection data, but also provide independent

coordinate determination for objects detected by the NOAO PDS. Table 2 lists the number and percent of the total of optical counterparts classified by eye as stellar or galaxian which were seen around SSC sources from all 53 AOs, broken down for 60 μm-only and all other sources. These data show that 363 of the 927 SSC sources were optically identified as stellar or galaxian. Note that of the 109 60 μm-only sources which were bright enough to identify, 94 were identified as galaxies. Many of these galaxies were very faint edge-on spirals.

3. Examination of Cirrus over each AO

The IRAS PSC contains a large number of 100 μm-only detections (33,195 sources or 13.5% of the entire catalog) which have been closely correlated with knots in galactic cirrus (Low *et al.* 1984). Since cirrus emission is strongest at 60 and 100 μm, cirrus knots were suspected as the cause of the surplus of 60 μm sources in the SSC. Although cirrus emission peaks at 100 μm and should also be detected in that band, the sensitivity of the SSC is much better at 60 μm than it is at 100 μm (120 *vs.* 440 mJy, respectively) and faint cirrus might be detectable only at 60 μm rather than in both bands. Smooth cirrus would not have been detected as a point source in either catalog; only clumps would appear point-like.

Table 2

RESULTS OF MANUAL METHOD OF CLASSIFICATION

Classification by Visual Inspection of Slides for
927 SSC Sources contained in 53 AO Grids

Visual Inspection Classification	Number of Sources	Percent of 923	60μm-only Sources	All Other Sources
Galaxies (G)	226	24.5	94	132
Stars (S)	137	14.8	15	122
No ID (F,M)	456	49.4	233	223
Empty fields (B)	104	11.3	46	58
Total viewed	923	100.0	388	535
Sources not viewed	4	0.4	1	3

Each AO field was visually examined on the 60 and 100 μm IRAS Sky Flux plates (IRAS Sky Brightness Images 1988) to assess the degree of cirrus contamination present. If most of the 60 μm-only sources in a field were optically *un*identifiable and the Sky Flux photographs showed heavy cirrus contamination, it could indicate that these 60 μm-only sources are unlikely galaxian point sources.

A scale of 0 to 5 was chosen subjectively to span the range of absent to heavy cirrus contamination, respectively, over the area of each AO field. A cirrus index of 0 reflects no detectable cirrus and an index of 5 indicates a plate which was opaque essentially due to cirrus. Figure 8 contains the 100 μm cirrus index *vs.* the density of 60 μm detections for each AO field, in units of detections per deg^2. The 53 dense AOs of this study are plotted as open squares, and 14 AOs of the lowest 60 μm density are plotted as closed squares for comparison. This plot shows that cirrus does not appear to contribute to the 60 μm density of an AO field. From these data, we conclude that cirrus is not a likely cause of the high number of 60 μm detections in the SSC. Note that for every AO the cirrus contamination present at 60 μm was much less evident than that present at 100 μm.

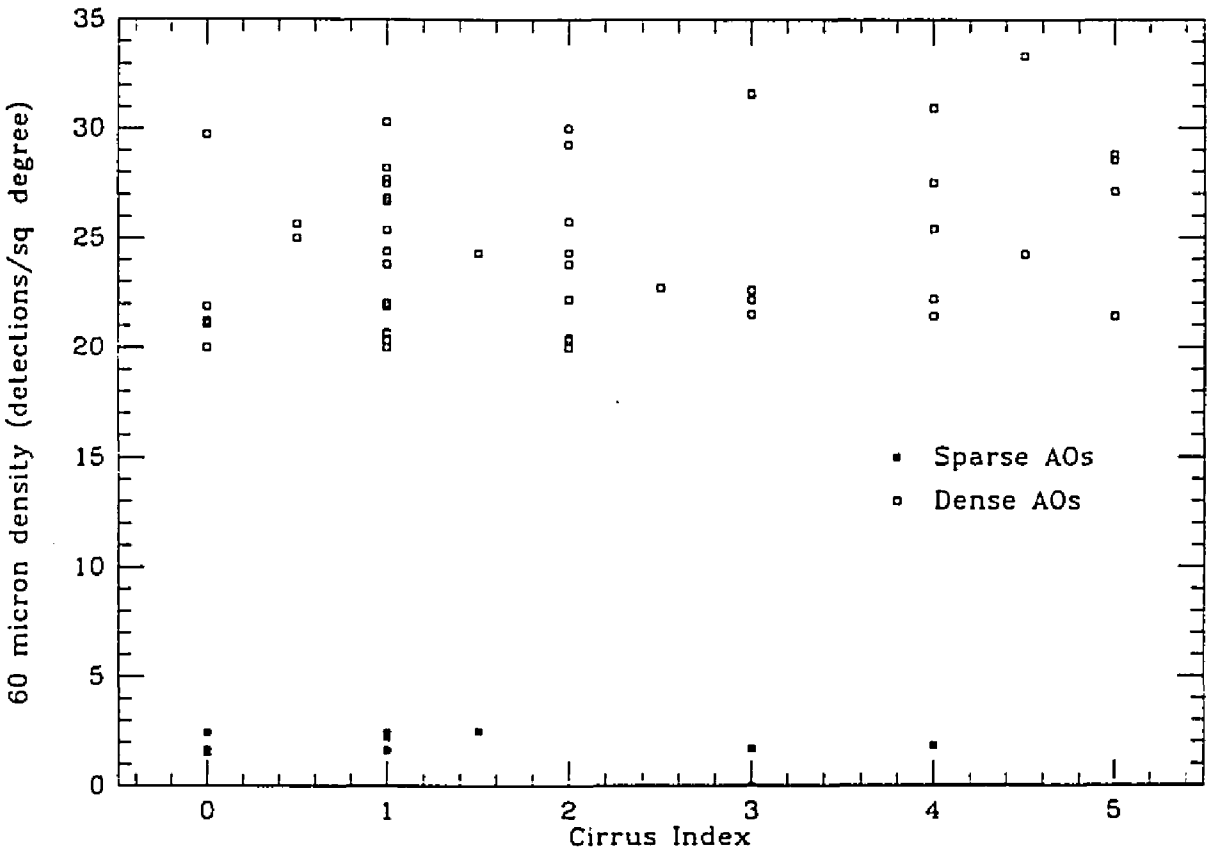

Figure 8. Plot of the cirrus index *vs.* the density of 60 μm detections for 54 AO fields with high 60 μm detection density (plotted as open squares) and 14 low density or sparse fields (plotted as filled squares). There appears to be no increase in the number of 60 μm detections in an AO for higher cirrus indices.

III. OPTICAL IDENTIFICATION OF IRAS SSC SOURCES

A. Probabilistic Matching of PDS Optical Candidates to SSC Sources

In order to identify IRAS SSC sources as being either stellar or galaxian and to study their optical characteristics, the optical counterparts to the IR sources must be found. Since there were many candidate optical sources found by the PDS near each SSC position (typically 2 to 5 optical sources per SSC source), a probabilistic source matching scheme was devised by R. Cutri (priv. comm.) to ascertain which optical source was the most likely counterpart to each SSC source. Modifications to the method were made by the author and D. Clemens (priv. comm.). Estimated association probabilities, based on positional differences and optical (PDS) magnitudes, were computed for each of the optical sources found within the appropriate error box for each IRAS source; these computations are discussed in section 2 below. The optical characteristics of the most likely counterparts found are discussed in the next chapter.

The output files from the PDS scanning effort contain information about all celestial objects found on the POSS or ESO plates by the PDS. In these files there

exist two populations of objects: 1) the optical counterparts to the IRAS SSC sources, and 2) everything else (the unrelated background population objects which are bright enough to appear on the plates). The term 'background population' is not meant to imply that the objects are more distant than the IRAS objects; it refers simply to the non-IRAS component which dominates and contaminates the PDS error boxes.

The optical sources found within the error box around each SSC source were identified as stellar or galaxian by the PDS parameters described in section II E 1 above. Each of these optical counterpart candidates was assigned a probability of being the optical counterpart to the SSC source. This probability contains two components: 1) a positional probability based on the positional offset of the optical source relative to the SSC source; and 2) a probability that an optical source of a given magnitude is not a member of the background sample of similar magnitude objects. Although the association probability computed assumes that there exists no more than one true optical counterpart to each IR source, it allows for the possibility that no optical counterpart was (or ought to have been) detected.

PDS output data files contain 10,000 to 20,000 optical objects per IRAS AO

field area, depending on the size of the AO field and the density of celestial objects within the AO field. Since there is a large variation in the source density from AO field to AO field for different parts of the sky, the background source density calculations were performed for each AO field independently; variations across the area of any particular AO field were deemed negligible.

1. Positional Probability

The first component of the association probability is based on the positional differences between the SSC source and each optical candidate. The distribution of positional errors of SSC sources, as found by comparing IRAS positions for bright stars and galaxies, may be approximated by two separate Gaussian functions, one for the in-scan and one for the cross-scan directions (KCYLG). The 1-σ error box dimensions for sources detected in the 12 and 25 μm bands are 4″ for the in-scan direction and 15″ for the cross-scan direction; for sources seen only in the 60 and 100 μm bands, these dimensions are 8 and 20″ (R. Cutri priv. comm.). Rectangular search boxes of $\pm 3\sigma$ size oriented along the proper (IRAS) scan directions for each AO field were used to cull optical counterpart candidates from the PDS output files for each SSC source. If detected fluxes of an SSC source spanned 12/25 and 60/100

μm, the smaller (12, 25 μm) search box was used. As many as 10 optical counterpart candidates were detected by the PDS inside search boxes around some SSC sources. Since the IRAS in-scan and cross-scan directions, i and c, respectively, have different error sizes, the equatorial positional differences between each IRAS source and the candidate optical sources had to be converted into in-scan and cross-scan positional differences. This was done via a rotation of the equatorial coordinate system into i and c by the tabulated inclination angle (the angle East of North by which the AO field was oriented on the sky; see Figure 1) of each AO.

An estimated gaussian positional probability, G, was computed for each optical counterpart candidate from the in-scan and cross-scan positional differences δi and δc, respectively, between the SSC source position and the optical (PDS) position according to

$$G(\Delta i, \Delta c) = exp\frac{-(\Delta i^2 + \Delta c^2)}{2} \tag{4}$$

where the argument of the exponent has been scaled using

$$\Delta i = \frac{\delta i}{\sigma_i} \tag{5}$$

and

$$\delta i = i_{SSC} - i_{PDS}. \tag{6}$$

A similar pair of expressions exists for c. The general effect of this probability is to favor more heavily optical candidates which are closer to the SSC source. The positional errors from PDS astrometry of the optical sources were ignored since they are typically about $1''$ (*i.e.*, much smaller than 1σ in the i or c directions).

2. Magnitude-related Probability

The second component of the association probability is based on the optical brightness of each candidate. The probability that a source of given optical brightness is the true IRAS source is related to the optical surface density function of the AO as a whole.

A Poisson probability, $P(m,q)$, gives the probability of finding m sources of a given magnitude within a search box when q (the average number of) optical sources are expected. It is defined as

$$P(m,q) = \frac{q^m}{m!}e^{-q} \tag{7}$$

where m is always an integer and q is most often not. The qs for each magnitude bin were empirically determined for each AO field. From the qs, we know what background population configurations are most likely to appear in each search box. From Equation 7 and the surface density function of the AO, we estimate the

probability of a certain background configuration.

For each AO, all of the optical sources detected by the PDS (some 10,000-20,000) were sorted into magnitude bins of width 0.5 PDS mag. PDS magnitudes were used rather than CCD ones so that none of the errors from the PDS-CCD conversion were introduced. Half-magnitude bins were used because 0.5 PDS mag corresponds to at least two times the intrinsic magnitude scatter over the magnitude range of the PDS-CCD conversion. A 'completeness limit', defined as the PDS magnitude bin containing the largest number of sources, was obtained, and all sources fainter than that limit were discarded. The remaining sources were used to construct a surface density function for the AO field. As an example, Figure 9 shows the magnitude histogram for AO field 9454, which exhibits a completeness limit of 12.5 PDS mag.

For the optical sources within an AO field brighter than the completeness limit, the number of optical sources in each half-magnitude bin was found: n_i optical sources in the ith magnitude bin. That total number, n_i, was divided by the number of search boxes (defined in section 1 above) which would cover the optical scan area, giving the mean expected number of optical sources, q_i, within a search

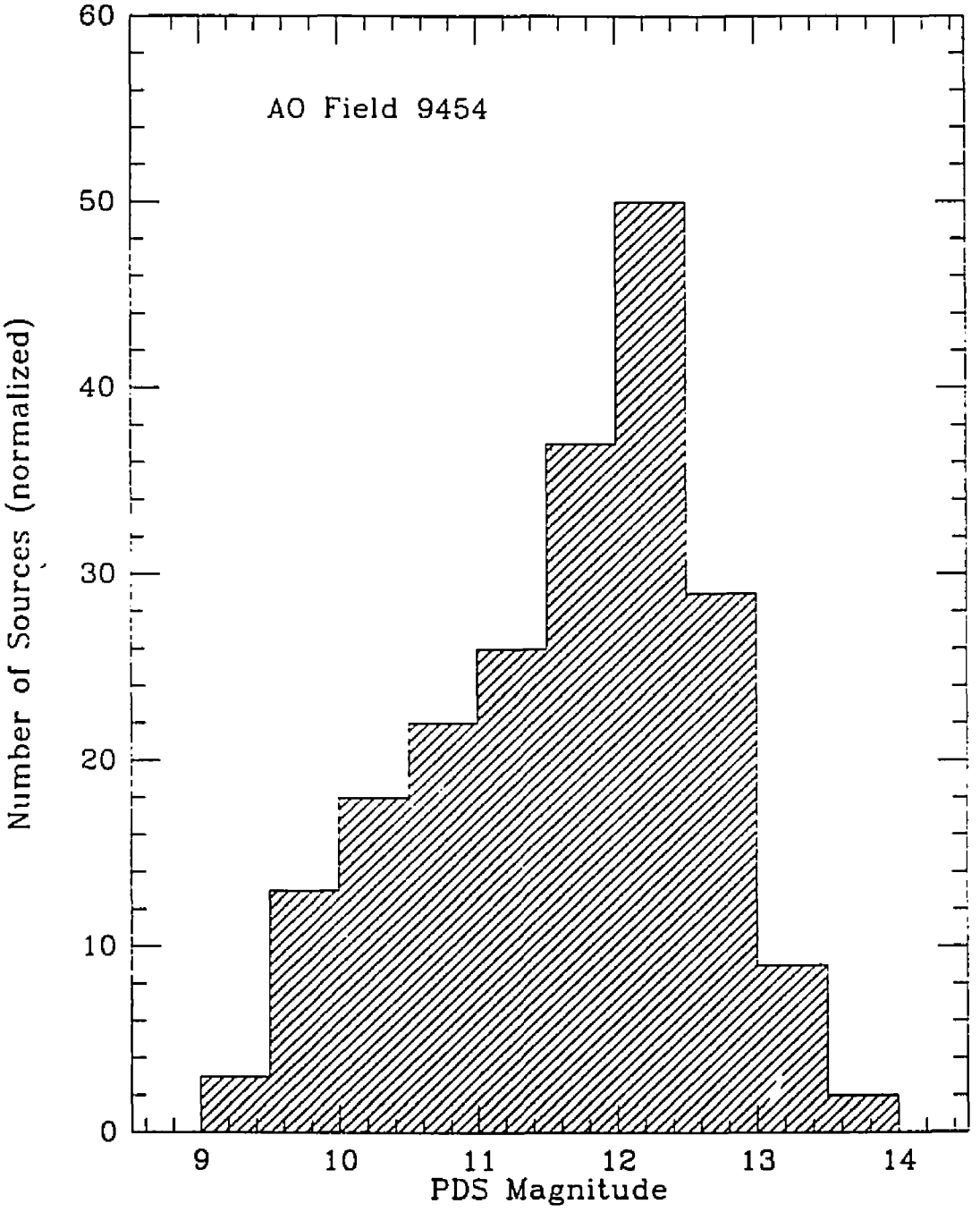

Figure 9. Histogram of the PDS magnitudes in AO field 9454, normalized by the total amount of sources in the field. The number of sources within a magnitude bin increases until 12.5 PDS mag, the completeness limit. All sources dimmer than 12.5 PDS mag were discarded when the field was studied.

box area for magnitude bin i. These q_i make up the surface density function for each AO. Two major assumptions were made: 1) there is only one optical counterpart to the IRAS source, and 2) there exist two populations of objects in the sky: the IRAS optical counterparts and the (unrelated) background population.

Let us now discuss what happens within a search box. There are typically three to five optical counterpart candidates found around each SSC source. We want to know what the probability is that each source individually could be the optical counterpart to the IRAS source. We would also like to know what the probability is that the IRAS source was or was not detected at all. We take one specific source out of the candidate list then compute the likelihood of finding a background configuration made up of the remaining sources. The likelihood of such a background configuration becomes the relative probability that the removed optical source is the optical counterpart to the IRAS source, based on its magnitude and the surface density function of the AO. The same probability, defined as $I(P)$, is calculated separately for all optical sources inside the search box. Since $I(P)$ is calculated for each AO and SSC source, it is not an absolute probability but a relative one.

Consider the following example of a computation of $I(P)$. It is a function of Poisson probabilities as defined in Equation 7. There is one $P(m,q)$ for each magnitude bin represented by the optical sources. An additional $P(m,q)$ is computed for the possibility that the IRAS source was not listed as one of the optical sources within the search box. Suppose that the PDS detected sources in each of three, N, magnitude bins, such there are m_1, m_2, and m_3 sources in bins 1, 2, and 3. (There will be $m_1 + m_2 + m_3$ optical sources.) Recall that the average number of background sources per IRAS error box in the three bins will be q_1, q_2, and q_3, respectively. Since there is at most one optical counterpart, there are $N + 1$ cases to consider: one for each magnitude bin (*i.e.*, the counterpart is a member of that magnitude bin) plus the non-detection case. The probability of occurrence of a particular case is labeled C_i. The probability of a particular case C_i will be constructed from the product of probabilities $P_i(m,q)$ computed for each magnitude bin used to construct the surface density function of the AO. In other words, we include the $P(m,q)$ for the bins where m is zero. For the case of an optical counterpart from a specific bin, m_i is decreased by one for that bin, since $m_i - 1$ optical sources are part of the background population and one is the optical counterpart to the IRAS

source. For the case of no optical counterpart detected, we have the same product of $P(m,q)$, but none of the bins have removed sources. Let $\prod_i P_i(0,q_i)$ denote the product of the bins which have no detected sources. All possible background configurations can be expressed as follows:

$$\text{IRAS source in bin 1} : C_1 = P_1(m_1-1,q_1)P_2(m_2,q_2)P_3(m_3,q_3)\prod_i P_i(0,q_i)$$

$$\text{IRAS source in bin 2} : C_2 = P_1(m_1,q_1)P_2(m_2-1,q_2)P_3(m_3,q_3)\prod_i P_i(0,q_i)$$

$$\text{IRAS source in bin 3} : C_3 = P_1(m_1,q_1)P_2(m_2,q_2)P_3(m_3-1,q_3)\prod_i P_i(0,q_i)$$

$$\text{No IRAS source seen} : C_4 = P_1(m_1,q_1)P_2(m_2,q_2)P_3(m_3,q_3)\prod_i P_i(0,q_i)$$

$I(P)$ is normalized by all the cases:

$$\sum_{i=1}^{N+1} C_i(P) \tag{8}$$

In the above example, *each* source in bin 2 has the same probability of being the optical counterpart to the IRAS source, normalized by the total number of candidates found in that bin, m_2. For example, the probability that the IRAS source is in bin 2 is

$$I_2(P) = \frac{P_1(m_1,q_1)P_2(m_2-1,q_2)P_3(m_3,q_3)\prod_i P_i(0,q_i)}{m_2\sum_{i-1}^{N+1} C_i(P)} \tag{9}$$

Note that the $\prod_i P_i(0, q_i)$ factor cancels out when we normalize $I(P)$. Therefore, we need only consider the magnitude bins from which optical sources were detected.

a. Behavior of the Magnitude-related Probability

In general, brighter sources will have higher $I(P)$s. Consider an SSC search box within which sources of the same magnitude were found. Suppose q for this bin is 1.3; let us vary m and see what happens to $I(P)$. This is done in Table 3. $I(P)$ in the table is the probability that any one of the m sources is the counterpart; they have equal probability since they are the same magnitude. Note that as m increases, our ability to pick which source is the IRAS optical counterpart decreases, but the probability that we have detected the optical counterpart increases. If there were a brighter source detected, its q would be lower, so the $I(P)$ would be higher. The sum of the $I(P)$ of all optical sources in a search box equals the probability that the IRAS source was detected. The complement of that probability is the probability that the optical counterpart to the IRAS source was not detected. A counterpart may not have been detected because it was outside the boundaries of the search box, or it was dimmer than the optical completeness limit of the AO.

b. Example Computation of the Magnitude-related Probability

Table 3

BEHAVIOR OF I(P) FOR VARIOUS m OF THE SAME MAGNITUDE

m	I(P) (for each source)	Nondetection Probability
0	0	1
1	0.435	0.565
2	0.303	0.395
3	0.232	0.303

Table 4, which will be discussed in detail in section B below, lists the SSC sources (in RA order) and all optical counterpart candidates within each error box found by the PDS which are above the completeness limit. Column 8 of the optical data lists the Poisson probability $I(P)$ for each optical source. Let us go through the computation of $I(P)$ for SSC source 04397-4318 from Table 4. There are two magnitude bins from the four listed sources: bin 1 contains two 10.3 PDS mag source and bin 2 contains the 12.4 and 12.1 PDS mag sources. The ms and qs for this source are:

$$m_1 = 2 \quad and \quad q_1 = 0.16992$$

$$m_2 = 2 \quad and \quad q_2 = 0.48525$$

For the sources in bin 1 (the 10.3 mag sources),

$$I_1 = \frac{P_1(m_1 - 1, q_1)P_2(m_2, q_2)}{P_1(m_1 - 1, q_1)P_2(m_2, q_2) + P_1(m_1, q_1)P_2(m_2 - 1, q_2) + P_1(m_1, q_1)P_2(m_2, q_2)} \tag{10}$$

Filling in the ms,

$$I_1 = \frac{\frac{q_1 q_2^2}{2}}{\frac{q_1^2 q_2}{2} + \frac{q_1 q_2^2}{2} + \frac{q_1^2 q_2^2}{4}} \tag{11}$$

and filling in the qs,

$$I_1 = 0.6968, \tag{12}$$

Table 4

PDS Optical Source Matches to IRAS SSC Sources

SSC Name	RA (1950)	DEC (1950)	Δc (arcsec)	Δi (arcsec)	T(I,G)	CCD mag	I(P)	PDS mag		NB
AO Field 9454										
04381 − 4324	043809.7	−432443		−0.06	−0.07	0.14	0.35			M
	043808.9	−432443	8.7	0.1	0.0691	19.8	0.0761	12.1		s
	043807.8	−432440	20.5	−3.8	0.0673	18.5	0.1277	11.1		x
	043814.0	−432437	−47.1	−2.2	0.0130	15.7	0.2172	10.3		a
	043812.7	−432454	−31.8	13.5	0.0074	19.3	0.1078	11.6		s
	043812.2	−432422	−28.6	−18.6	0.0053	15.9	0.2172	10.4		a
	043804.6	−432455	56.3	8.1	0.0025	14.8	0.2172	10.2		g
04382 − 4332	043817.1	−433220		−0.06	−0.07	−0.10	0.32			M
	043819.0	−433230	−19.9	11.7	0.0459	17.4	0.2199	10.7		s
	043815.2	−433203	19.4	−18.1	0.0149	14.3	0.3095	10.1		a
	043815.2	−433202	19.4	−19.2	0.0109	15.3	0.3095	10.3		a
	043812.6	−433241	50.3	17.8	0.0004	20.0	0.1084	12.4		s
04383 − 4423	043819.9	−442317		−0.06	0.14	1.29	3.04			G
	043822.3	−442308	−26.2	−6.3	0.0569	18.5	0.9021	11.1		x
04384 − 4354	043828.5	−435400		−0.06	−0.07	0.14	−0.32		*	G
	043831.2	−435350	−29.8	−7.9	0.0586	15.9	0.2909	10.4		g
	043826.5	−435407	22.1	5.5	0.0439	20.0	0.1019	12.4		s
	043831.4	−435405	−30.9	7.8	0.0273	19.4	0.1444	11.7		s
	043825.5	−435419	33.7	17.1	0.0051	18.2	0.2067	11.0		s
	043832.3	−435415	−39.9	18.3	0.0020	17.3	0.2067	10.7		s
04385 − 4319	043833.9	−431944		−0.06	−0.07	0.09	−0.32		*	G
	043833.4	−431953	6.1	9.4	0.0500	19.8	0.1045	12.1		s
	043834.6	−431959	−6.5	16.4	0.0246	17.4	0.2119	10.7		s
	043837.3	−431940	−37.2	−0.6	0.0184	20.1	0.1045	12.5		s
	043834.5	−432001	−5.3	17.6	0.0181	17.5	0.2119	10.8		s
	043837.4	−431939	−38.4	−1.8	0.0161	20.1	0.1045	12.5		s
	043837.2	−431956	−35.0	15.3	0.0074	17.0	0.2119	10.6		s

Table 4 (*continued*)

SSC Name	RA (1950)	DEC (1950)	Δc (arcsec)	Δi (arcsec)	T(I,G)	CCD mag	I(P)	PDS mag	NB
04387 − 4339	043845.8	−433909		−0.06	−0.07	0.14	−0.32		* G
	043845.5	−433857	2.5	−11.3	0.0343	19.0	0.0935	11.4	s
	043849.0	−433921	−33.8	14.5	0.0313	13.2	0.6745	9.9	g
	043844.6	−433920	13.8	10.2	0.0196	19.8	0.0557	12.1	s
	043843.9	−433852	19.4	−18.3	0.0043	18.7	0.0935	11.2	s
	043841.1	−433910	51.0	−2.1	0.0021	19.8	0.0557	12.1	s
04387 − 4404	043847.8	−440457		−0.06	−0.07	0.10	−0.32		* M
	043846.5	−440454	13.8	−3.7	0.2051	15.1	0.2891	10.2	g
	043846.4	−440454	14.9	−3.8	0.1954	14.8	0.2891	10.2	g
	043849.1	−440453	−14.2	−2.4	0.0752	19.8	0.1013	12.1	s
	043848.4	−440514	−5.2	17.6	0.0146	18.7	0.1700	11.2	s
	043849.4	−440438	−18.5	−17.2	0.0066	20.1	0.1013	12.4	s
04388 − 4357	043851.1	−435736		−0.06	−0.07	0.09	−0.32		* M
	043851.8	−435727	−8.1	−8.0	0.0981	17.8	0.1768	10.8	s
	043853.9	−435732	−30.4	−1.5	0.0453	18.3	0.1463	11.0	s
	043848.2	−435738	31.4	−0.1	0.0361	19.5	0.1235	11.8	s
	043846.2	−435732	52.5	−7.2	0.0026	19.7	0.1235	12.0	s
	043850.8	−435758	4.8	22.1	0.0026	19.4	0.1235	11.7	s
	043846.9	−435754	46.5	15.0	0.0010	19.8	0.0872	12.2	s
	043855.6	−435750	−47.4	18.3	0.0008	17.3	0.1768	10.7	g
04389 − 4327	043857.6	−432754		−0.06	−0.07	0.18	0.42		S
	043900.0	−432807	−25.1	15.5	0.0304	11.3	0.4366	9.7	g
	043852.9	−432808	52.1	11.0	0.0057	13.4	0.4366	9.9	g
	043854.0	−432748	38.7	−8.7	0.0031	20.0	0.0361	12.4	s
	043901.6	−432734	−44.8	−16.4	0.0007	17.7	0.0732	10.8	x
04395 − 4409	043930.5	−440915		−0.06	−0.07	0.13	−0.32		* M
	043927.9	−440919	28.2	2.3	0.1827	17.8	0.5160	10.9	s
	043928.9	−440905	16.6	−10.3	0.1122	19.4	0.3604	11.6	s

Table 4 (*continued*)

SSC Name	RA (1950)	DEC (1950)	Δc (arcsec)	Δi (arcsec)	T(I,G)	CCD mag	I(P)	PDS mag	NB
04397 − 4349	043942.4	−434944		−0.06	−0.07	0.12	−0.32		* M
	043941.4	−434945	10.9	0.8	0.1260	19.6	0.1470	11.9	s
	043940.7	−434936	17.8	−8.7	0.0387	20.1	0.1037	12.4	s
	043940.7	−434935	17.7	−10.2	0.0312	20.0	0.1037	12.4	s
	043938.4	−434938	42.8	−8.6	0.0120	17.6	0.2105	10.8	g
	043938.4	−434937	42.7	−9.9	0.0100	17.8	0.2105	10.9	x
	043939.0	−435005	38.2	18.5	0.0020	18.7	0.1742	11.2	s
04397 − 4318	043945.0	−431834		−0.06	−0.07	−0.10	0.34		M
	043944.3	−431830	7.3	−4.3	0.2813	15.6	0.3484	10.3	g
	043944.3	−431828	7.3	−5.6	0.2547	15.5	0.3484	10.3	g
	043945.8	−431823	−9.4	−9.5	0.0542	20.1	0.1220	12.4	s
	043948.2	−431835	−34.8	3.5	0.0244	19.8	0.1220	12.1	s
04398 − 4316	043952.8	−431652		−0.06	−0.07	0.12	−0.32		*
	043952.0	−431651	8.7	−0.7	0.1018	19.9	0.1124	12.3	s
	043952.9	−431641	−1.8	−10.6	0.0942	17.2	0.2279	10.7	s
	043949.7	−431701	34.5	7.4	0.0337	17.9	0.2279	10.9	x
	043950.0	−431707	31.6	13.5	0.0130	18.6	0.1886	11.1	x
	043953.8	−431714	−9.4	22.7	0.0030	19.2	0.1886	11.5	s

as tabulated. Similarly for the bin 2 sources,

$$I_2 = \frac{P_1(m_1, q_1)P_2(m_2 - 1, q_2)}{P_1(m_1 - 1, q_1)P_2(m_2, q_2) + P_1(m_1, q_1)P_2(m_2 - 1, q_2) + P_1(m_1, q_1)P_2(m_2, q_2)} \tag{13}$$

Filling in the ms and qs and dividing by m_2, we obtain the probability for each optical source in bin 2,

$$I_2 \quad = \quad 0.2440 \tag{14}$$

Summing 0.1220 + 0.1220 + 0.3484 + 0.3484 and subtracting from 1 obtains 0.0592 as the probability of *not* having detected the optical counterpart to the IRAS source.

Note that although both of the bin 2 sources have the same magnitude-related probability of association with the IRAS source, they will quite likely have different positional probabilities which will result in different total association probabilities.

3. Total Association Probability

The total probability, $T(I, G)$, that an optical counterpart candidate is likely associated with a particular IRAS SSC source is the product of the magnitude-related and positional probabilities:

$$T(I, G) \; = \; I(P)G(\Delta i, \Delta c). \tag{15}$$

Column 6 of Table 4 lists the total association probability $T(I, G)$ for each optical source.

The method used here to determine the association probability of each optical counterpart candidate is based on the same criteria as those used by Prestage and Peacock (1983) in their optical identification program of radio sources. They use a likelihood ratio for each optical candidate, based on the optical magnitude of the candidate relative to the immediate background surface density function, and on the positional differences between the radio and optical sources. The likelihood ratio, like the association probability used here, is a relative measure since it uses the surface density function of the immediate area, not of the whole sky. When the likelihood ratio was computed for the optical candidates found around 14 of the SSC sources studied here, the ordering of the optical candidates by association probability or likelihood ratio was the same in all cases, with minor order changes between (*e.g.*,) the fourth and fifth candidate in the list around an SSC source.

The sum of the association probabilities of all of the optical counterpart candidates around each SSC source is the probability that the optical counterpart for that SSC source has been detected. Figure 10 contains histograms of the fraction

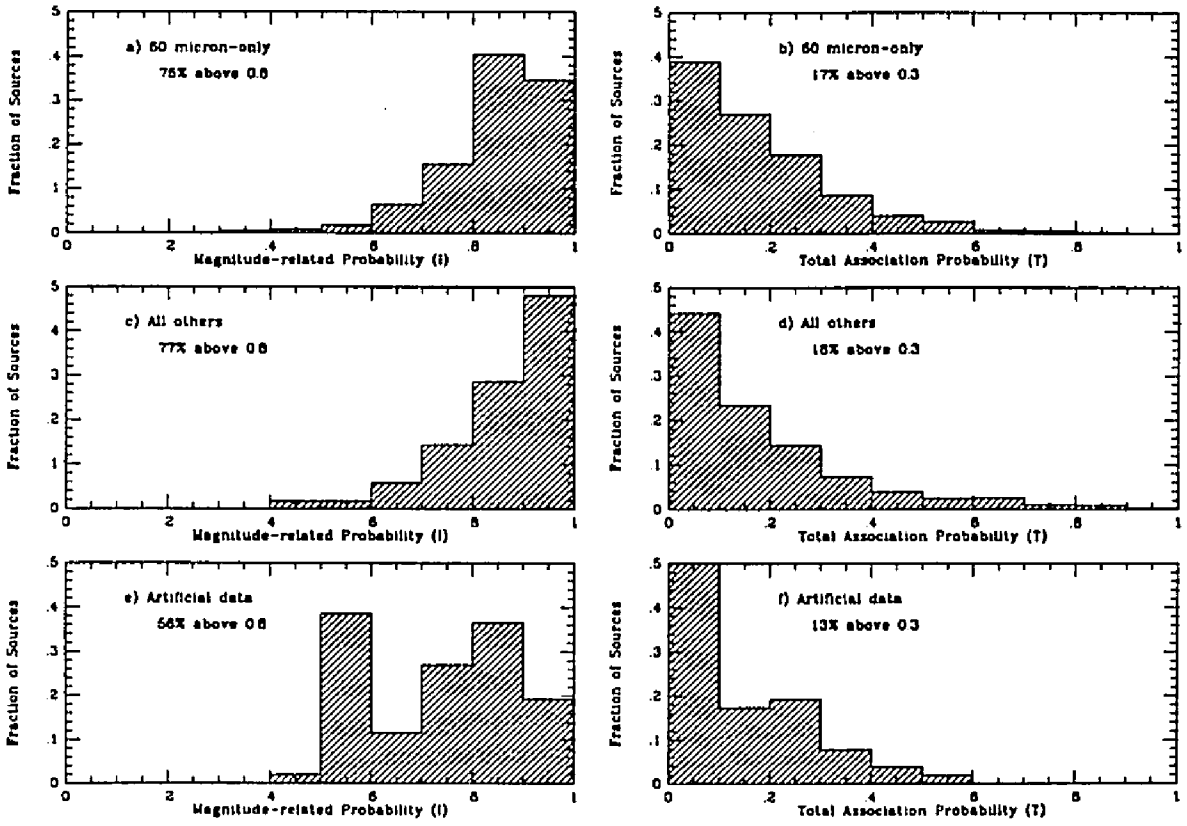

Figure 10. Histograms of the fraction of sources in bins of magnitude-related probability (a, c and e) and total association probability (b, d and f) for 60 μm-only, all other SSC sources and artificial sources. The fractions are based on the total number of sources of a given type of detection: 361 60 μm-only, 467 other sources, and 52 artificial sources. The percentages in the legends refer to the sources with probabilities above 0.3 or 0.8 as noted. In all cases, the 60 μm-only and all other SSC sources fared similarly to each other, and notably better than the artificial sources.

of SSC sources *vs.* probability. The figure contains six histograms which have 60 μm-only sources, all other sources and artificial data (see section III D), with the magnitude-related, I, or total association, T, probabilities. The fraction of each type of source is plotted: there are 361 60 μm-only, 467 other sources and 52 artificial sources. Figures 10a, c and e show that 75% of 60 μm-only sources, 77% of all other sources and 56% of the artificial sources have at least an 80% probability of having been detected, based on their magnitudes alone. Figures 10b, d and f show that 17% of 60 μm-only sources, 18% of all other sources and 13% of artificial sources have at least a 30% total association probability. Recall that although I is normalized so that all probabilities sum to unity for each SSC source (including the non-detection case), that is not so for the total association probability. In other words, the complement of the sum of the total association probabilities for each SSC source cannot be compared to the complement of the sum of the magnitude-related probabilities. They have more meaning when compared to the corresponding probabilities of the artificial sources. The selection and characteristics of the artificial sources will be discussed in section III D below.

B. Optical Counterpart to IRAS SSC Matches

Table 4 contains all of the IRAS SSC sources and their optical counterpart candidates which were found by the PDS within the error bars of each SSC position for AO field 10838. The table lists the SSC source name followed by its optical counterpart candidates, listed in order of total probability of association with the SSC source. An asterisk in the NB column denotes a 60 μm-only source. The tabulated IR data is the SSC name (column 1) and the RA and DEC, epoch 1950 (columns 2 and 3). Column 10, the NB column, also contains the identification of the optical counterpart from the visual inspection of slides: G denotes a galaxian object, S a stellar one, M indicates multiple faint objects, F means a single faint object, B indicates a visually blank field, and a blank indicates that the source was not viewed by eye. (Some of the sources were behind very bright foreground objects which blackened those areas of the plates). Optical counterparts are listed under the IR sources, in order of the total association probability. Columns 2 and 3 contain the (1950) Right Ascension and Declination; columns 4 and 5 contain the cross-scan and in-scan positional differences between the PDS and SSC coordinates, in arcsec; column 6 contains the association probability $T(I,G)$ as discussed in section A above; columns 7 and 9 contain CCD and PDS magnitudes, respectively; column 8

contains the background probability $I(P)$ also discussed in section A; and column 10 contains the classification of the optical source derived from the PDS parameters: g denotes a galaxian object, s denotes a stellar object, and a and x denote an ambiguous (unidentifiable) object, as discussed in section II E 1 and illustrated in Figure 7. The full data set (Table 4 for all 53 AO fields) will be made available by the author in a machine readable format upon request.

C. Verification of the Automated Method of Optical Counterpart-to-IRAS SSC Source Matches

The PDS found 2778 optical counterpart candidates around 828 of the 927 SSC sources scanned. This is an average of 3.4 optical candidates per IR source. Eight of the 9 repeat sources discussed in the Introduction had at least one optical counterpart candidate. Table 5 lists the identifications of the most probably associated optical counterpart found around 828 SSC sources. From this method, 89% of the sources scanned had at least one optical counterpart candidate; 76% of the candidates have been identified as galaxian or stellar. Table 5 shows that 306 of the 389 60 μm-only sources in the sample have been identified (79%). Also, 401 of the 538 all other sources have been identified (75%). These data show that

Table 5

RESULTS OF AUTOMATED METHOD OF CLASSIFICATION

Classification by PDS and Probabilistic Source Matching Technique
for 927 SSC Sources with the Highest Association Probability

PDS Classification	Number of Sources	Percent of 927	60μm-only Sources	All Other Sources
Galaxies (g)	251	27.1	86	165
Stars (s)	456	49.2	220	236
Classified total	707	76.3	306	401
Classified Percent			78.7	74.5
Faint (a)	86	9.3	40	46
Faint (x)	35	3.8	15	20
Unclassified Total	121	13.1	55	66
Non-blank fields	828	89.3	361	467
Blank fields	99	10.7	28	71
2778 optical counterpart candidates found by the PDS around 828 SSC sources				

identification of 60 μm-only sources is essentially the same as that for all others. This is in part due to the fact that the PDS does not easily identify very bright (*e.g.*, SAO stars) objects. The association probabilities of the most likely optical candidates will be studied in the next chapter to determine if they are significantly lower for 60 μm-only sources than they are for all other sources.

To verify the robustness of the automated method described in section A above, the 40% of the sources which were classified as stellar or galaxian (*i.e.*, as S or G) during the manual identification process were used to test the ability of the PDS to choose and classify optical counterparts (*e.g.*, as s or g). The optical counterpart candidate with the highest total association probability found by the PDS was compared to the object identified during the viewing of slides. Figure 11 contains histograms of the agreement between the PDS (automated) classification of objects and the visual inspection (manual) method binned by PDS magnitude. Only 361 sources were compared since they are the ones for which a definite classification was made (*i.e.*, S or G). Figure 11a contains a histogram for 105 60 μm-only sources and b) contains another for 224 Other sources. Figure 12 displays similar histograms, but the bins here are of 60 μm flux. The numbers on top of each bin

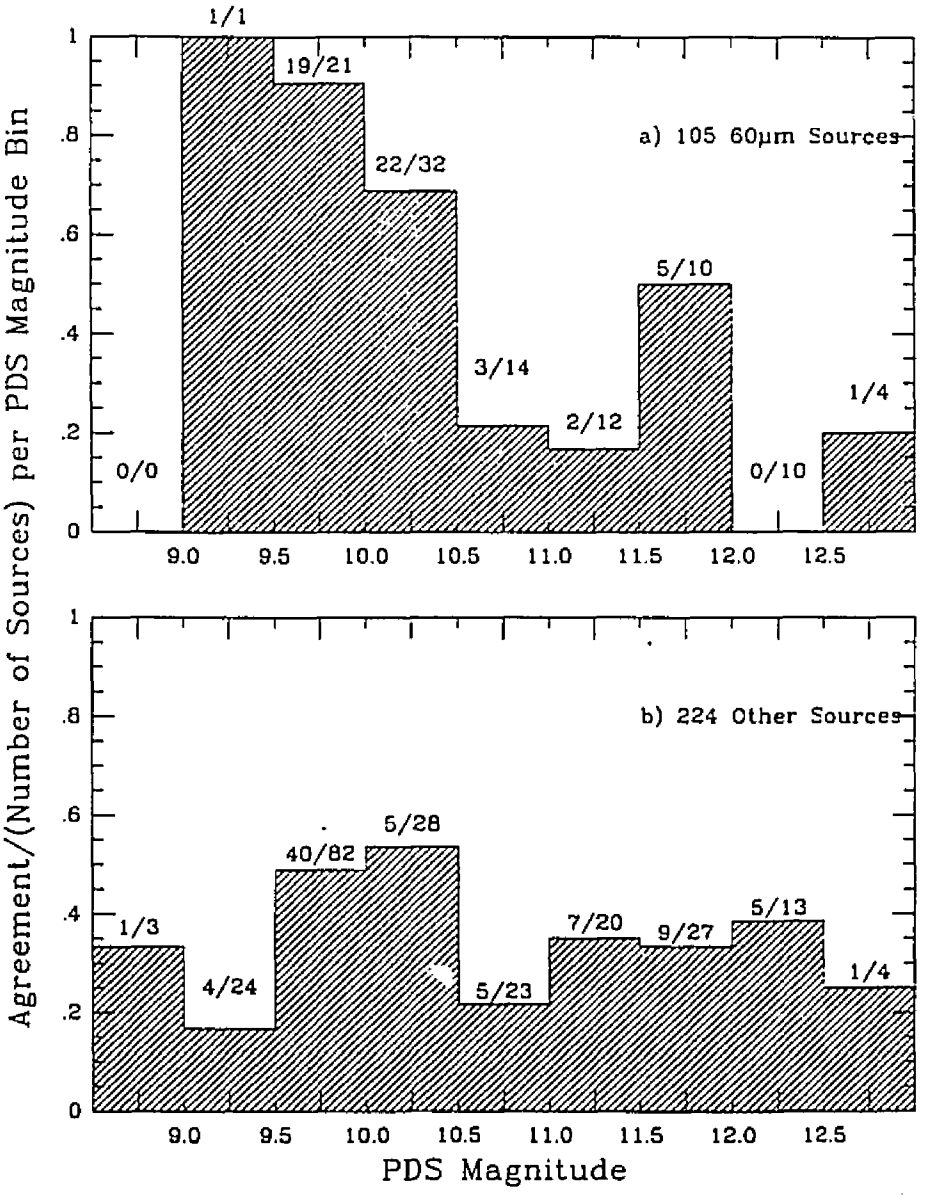

Figure 11. Histograms of the agreement between the automated and manual methods of classification of optical counterparts to SSC sources, binned by PDS magnitude. a) contains data for 60 μm-only sources and b) has all other sources. Agreement between the two methods is greatest for brighter objects. The numbers on top of each bin show how many sources were classified as the same by both methods over the total number of sources within that magnitude bin. *e.g.*, in a), the third bin shows that 17 out of 20 sources agreed in classification as assigned by each method.

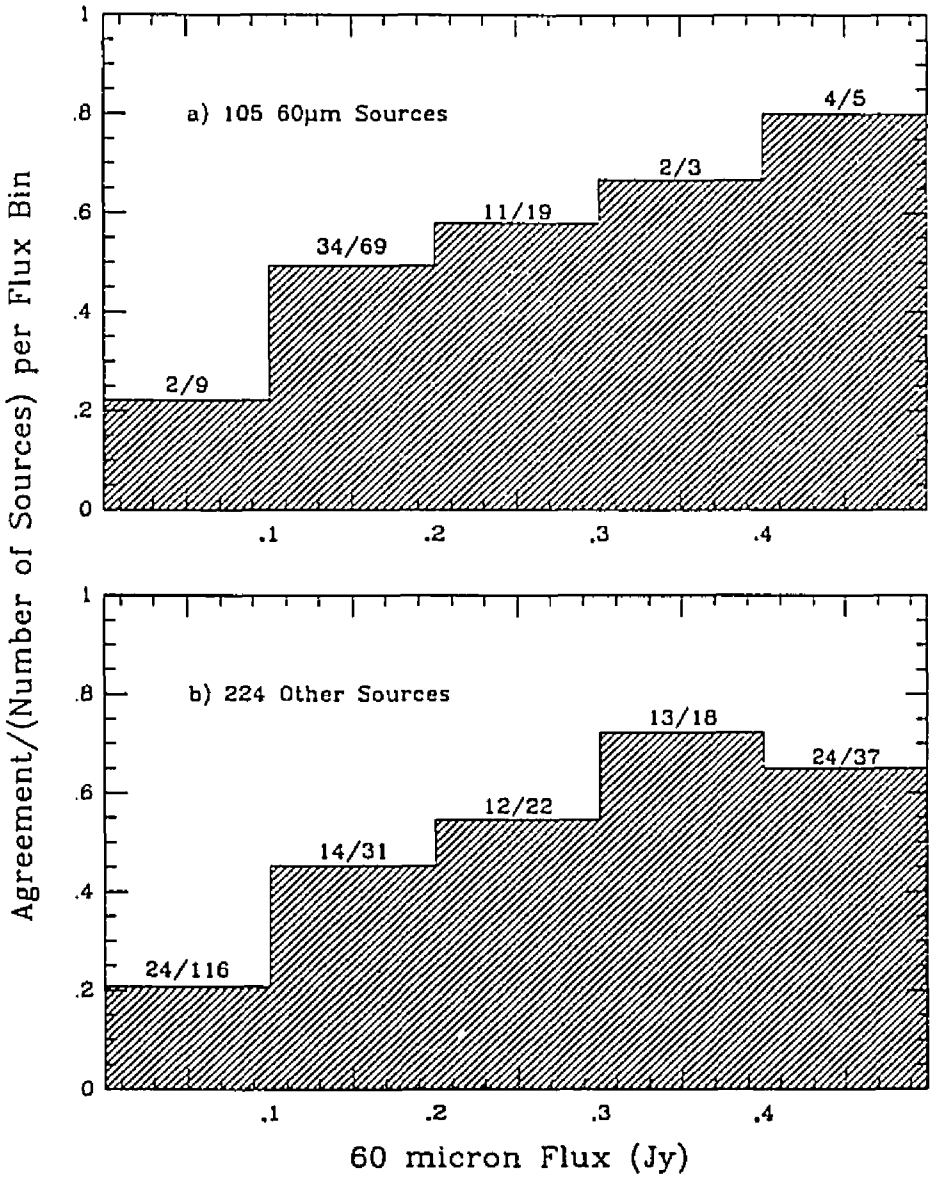

Figure 12. Histograms of the agreement between the automated and manual methods of classification of optical counterparts to SSC sources, binned by 60 μm flux. a) contains the data for 60 μm-only sources and b) contains the data for all other sources. As in Figure11, agreement is best at higher fluxes.

are the number of agreed sources *vs.* the total number found in that bin. It is evident from Figures 11 and 12 that agreement between the manual and automated methods worked best for brighter objects. Note that only 5 out of 24 Other sources in PDS mag bin 9.0 to 9.5 agree; this is probably due to the presence of bright stars which have diffraction spikes and do not appear round, as discussed in section II E 1. Nonetheless, it appears that when objects are bright enough for the manual and automated identification methods to be reliable, these methods agree well with one another.

D. Optical Counterparts of a Random Sample of Artificial Data

A sample of 67 artificial 60 μm-only sources were analyzed using the automated identification method to see how their characteristics compared to those of the optical counterpart candidates found around the SSC sources. The optical scan area of each AO was larger than the IRAS-scanned area. The artificial data were placed at random within the optical margin of the dense AO fields away from SSC sources and SAO stars. This area was not scanned by IRAS. All of the artificial sources were given 60 μm-only fluxes to immitate the differential Log N - Log F curves of the SSC subset, shown in Figure 4.

The results of the artificial data are presented in Table 6. There were 111 optical sources found inside the error boxes of 52 of the 67 artificial sources. This is an average of 2.1 optical sources per IR source. The percentage of PDS blank fields was higher for the artificial data (22%) than it was for the SSC sources (12%). Since bright objects were avoided when the artificial data were selected, blank fields are more likely due to the absence of objects. The most probably associated objects were stellar or unidentifiable as classified by the PDS. One of the most probable optical counterparts was galaxian. Table 6 shows that 63% of the artificial sources had stellar classifications. Comparison with the results of the SSC source classifications in Table 5 shows that 79% of the optical counterparts to 60 μm-only SSC sources were classified as galaxian or stellar. Finally, the average number of optical sources found around IR sources was 3.4 for the SSC sources and 2.1 for the artificial data. The SSC sources appear to have one extra optical source associated with them than do randomly placed artificial sources; most likely the IRAS optical counterpart.

The optical charateristics of the 2778 optical counterpart candidates found around 828 of the SSC sources will be explored in the next chapter. They will be compared to the optical characteristics of the artificial data as well.

Table 6

AUTOMATED METHOD OF CLASSIFICATION ON ARTIFICIAL DATA

Classifications of 67 Randomly-Placed Sources with the Highest Association Probability

PDS Classification	60μm-only Sources	Percent of 67
Galaxies (g)	1	1.5
Stars (s)	42	62.7
Classified total	43	64.2
Faint (a)	9	13.4
Faint (x)	0	0.0
Unclassified Total	9	13.4
Non-blank fields	52	77.6
Blank fields	15	22.4
111 optical counterpart candidates found by the PDS around 52 Non-SSC sources		

IV. OPTICAL CHARACTERISTICS OF IRAS SSC SOURCES

A. Comparison with Sources from the IRAS PSC

1. (B−60) Colors

Since galaxies are the predominant emitters of far-infrared radiation characterized by a 60 μm peak, a similarity between the 60 μm-only sources in the SSC and known galaxies in the PSC may exist. All entries from the *Cataloged Galaxies and Quasars Observed in the IRAS Survey* (Lonsdale *et al.* 1989) which had 60 μm-only emission, reported B magnitudes and which were at galactic latitudes $|b^{II}| \geq 30°$ were selected for comparison with the 60 μm-only sources in the SSC subset studied here.

The one optical counterpart candidate for each SSC source possessing the highest association probability (see Table 4) was used in the comparison. The B magnitudes for the SSC sources were estimated from the PDS-CCD conversion described in section II D.

The 60 μm fluxes, $F(60)$, of the SSC and PSC sources were converted to 60

μm magnitudes, M_{60}, using

$$M_{60} = 2.5\ log_{10}\left(\frac{F_0(60)}{F(60)}\right) \tag{16}$$

where

$$F_0(60) = 1.19\ \text{Jy} \tag{17}$$

(IRAS Explanatory Supplement 1988). Figure 13 contains plots of the (B−60) colors *vs.* a) the log of the 60 μm flux and b) the blue magnitude for optical counterparts to the SSC and PSC sources. The 204 PSC galaxies are plotted as filled squares, SSC optical counterparts classified by the PDS as galaxian are plotted as open squares and stellar objects are plotted as open stars. Half of the PSC galaxies have been typed. Ninety percent of those typed are spirals. From Figure 13a it is evident that the SSC 60 μm fluxes are lower than those of the PSC sources, due to the better sensitivity of the SSC in that band. These plots imply that SSC galaxian objects are probably faint spiral galaxies.

Figure 14 shows the same parameters as Figure 13, but it also includes quasars identified in the SSC from the Catalogue of Quasars and Active Nuclei (Véron-Cetty and Véron 1989) which have 60 μm-only detections in the SSC and known carbon stars and S stars (not all of which are 60 μm-only detections) also from the SSC.

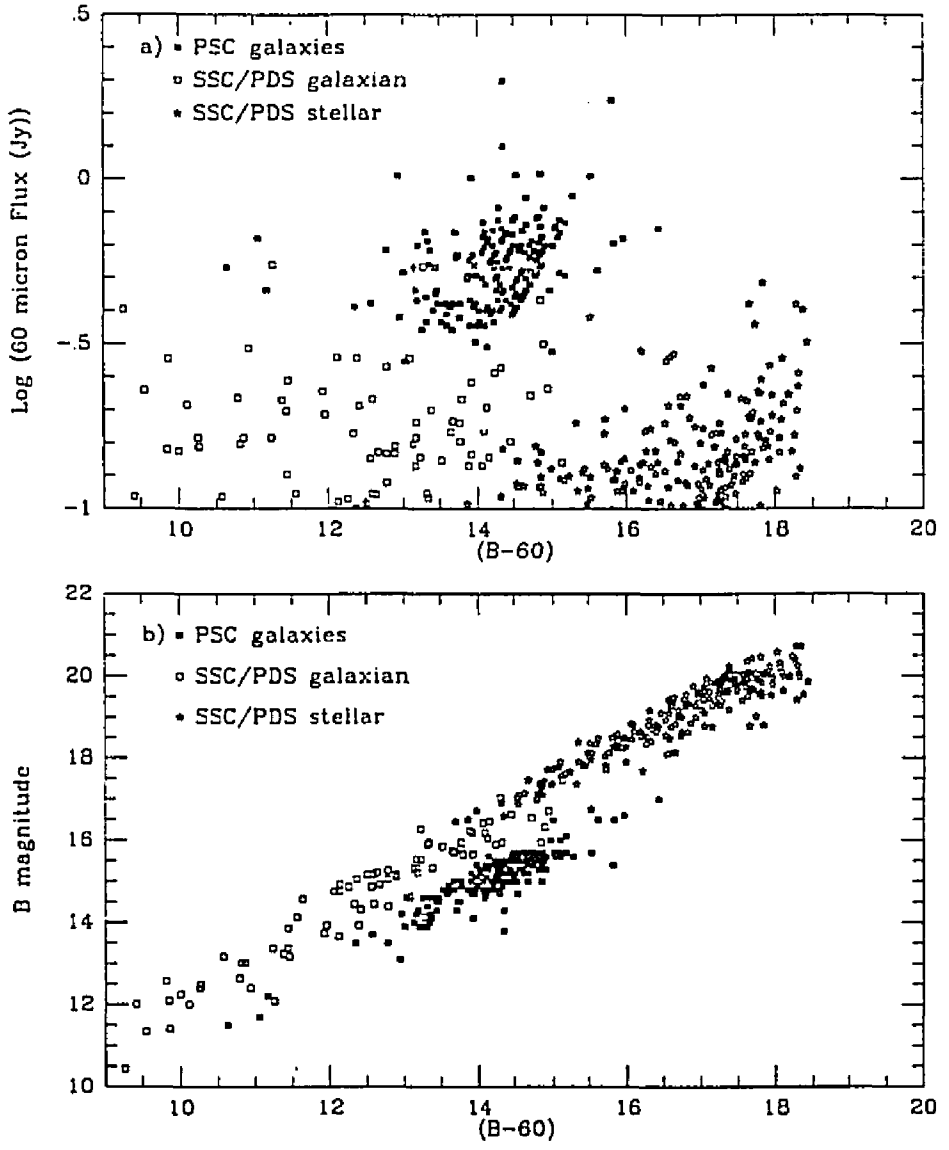

Figure 13. (B−60) color *vs.* a) log of the 60 μm flux (Jy) and b) blue magnitude for 204 galaxies from the PSC (plotted as closed squares) and optical counterparts to the SSC sources classified by the PDS as galaxian (plotted as open squares) and stellar (plotted as open stars). About half of the PSC galaxies have reported types; 90% of these are spirals. All sources on this plot are 60 μm-only sources at latitudes above $|b^{II}| \geq 30°$ from either catalog. The objects classified as galaxian by the PDS have similar colors to the galaxies from the PSC, but at fainter 60 μm fluxes.

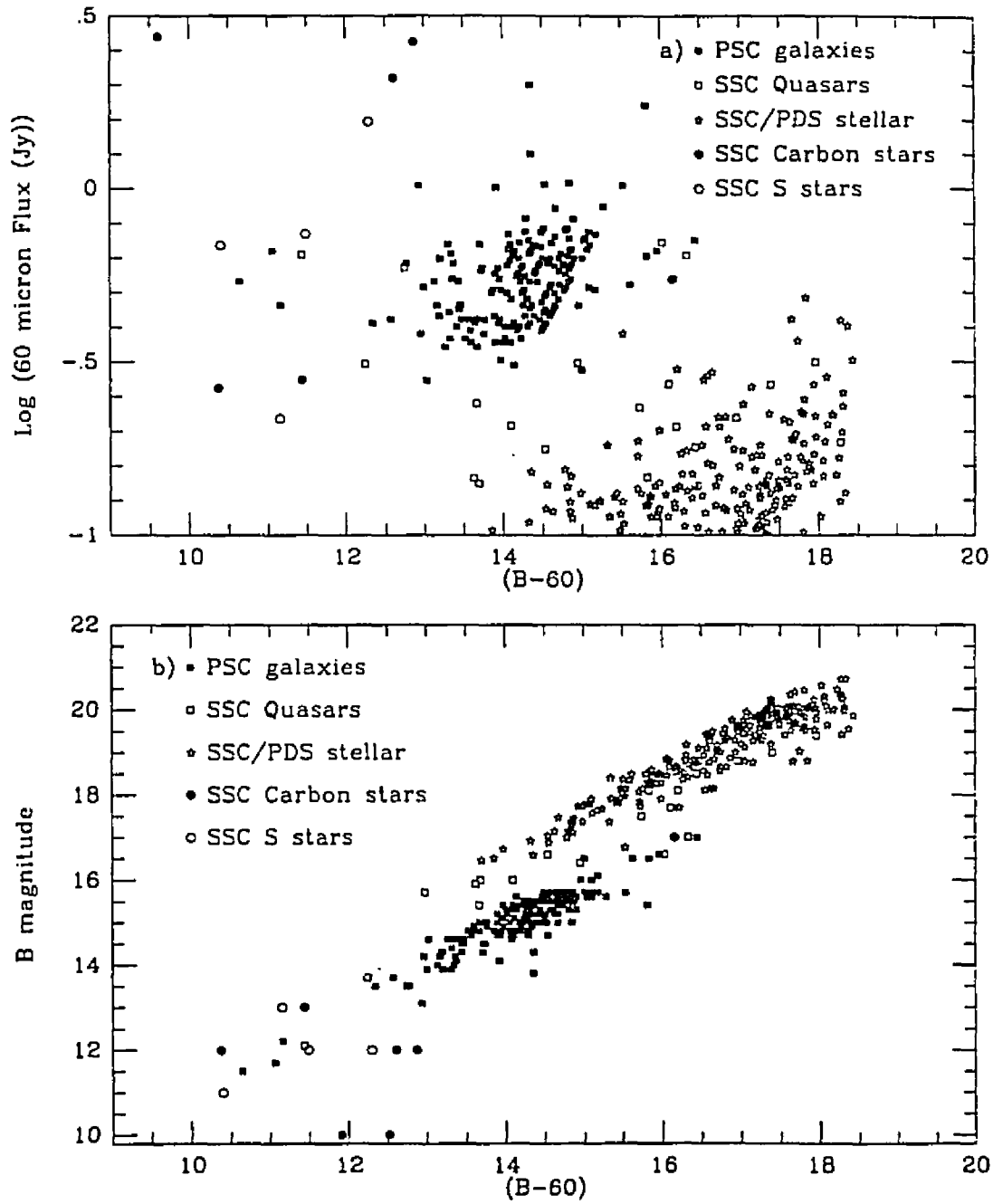

Figure 14. (B−60) color *vs.* a) log of the 60 μm flux (Jy) and b) blue magnitude for 204 galaxies from the PSC (plotted as closed squares) and other types of objects which are associated with SSC sources in the SSC catalog. Quasars are plotted as open squares, SSC stellar objects as open stars, SSC S stars as open circles, and SSC Carbon stars as closed circles. The SSC stellar objects most closely resemble the quasars.

The quasars seem to be in the same areas of the plots as the optical counterparts of the SSC sources classified by the PDS as stellar, and in the gap between the SSC stellar objects and PSC galaxies. The carbon and S stars do not fall in the same areas of the plot as the quasars or the PDS stellar objects. Note that these findings are in part due to the lack of very faint blue magnitudes for S and Carbon stars in the literature. From Figures 13 and 14, it appears that the stellar optical counterparts of SSC sources found and classified by the PDS are more likely quasars and not evolved stars.

Figure 15 displays the (B−60) colors of the PSC galaxies and the artificial data discussed in section III D. The optical counterparts here are not as well matched as those for the real SSC sources. There are no galaxian objects which are the most probably associated counterparts to the artificial 60 μm-only sources.

2. Comparison of PDS Classifications with PSC Catalog Associations

Another test of the validity of the PDS classification method is to compare the resulting classifications to those produced by an independent association scheme.

There are 101 sources in the SSC subset which are also listed in the PSC. Seventy of these sources have been positionally associated with objects contained

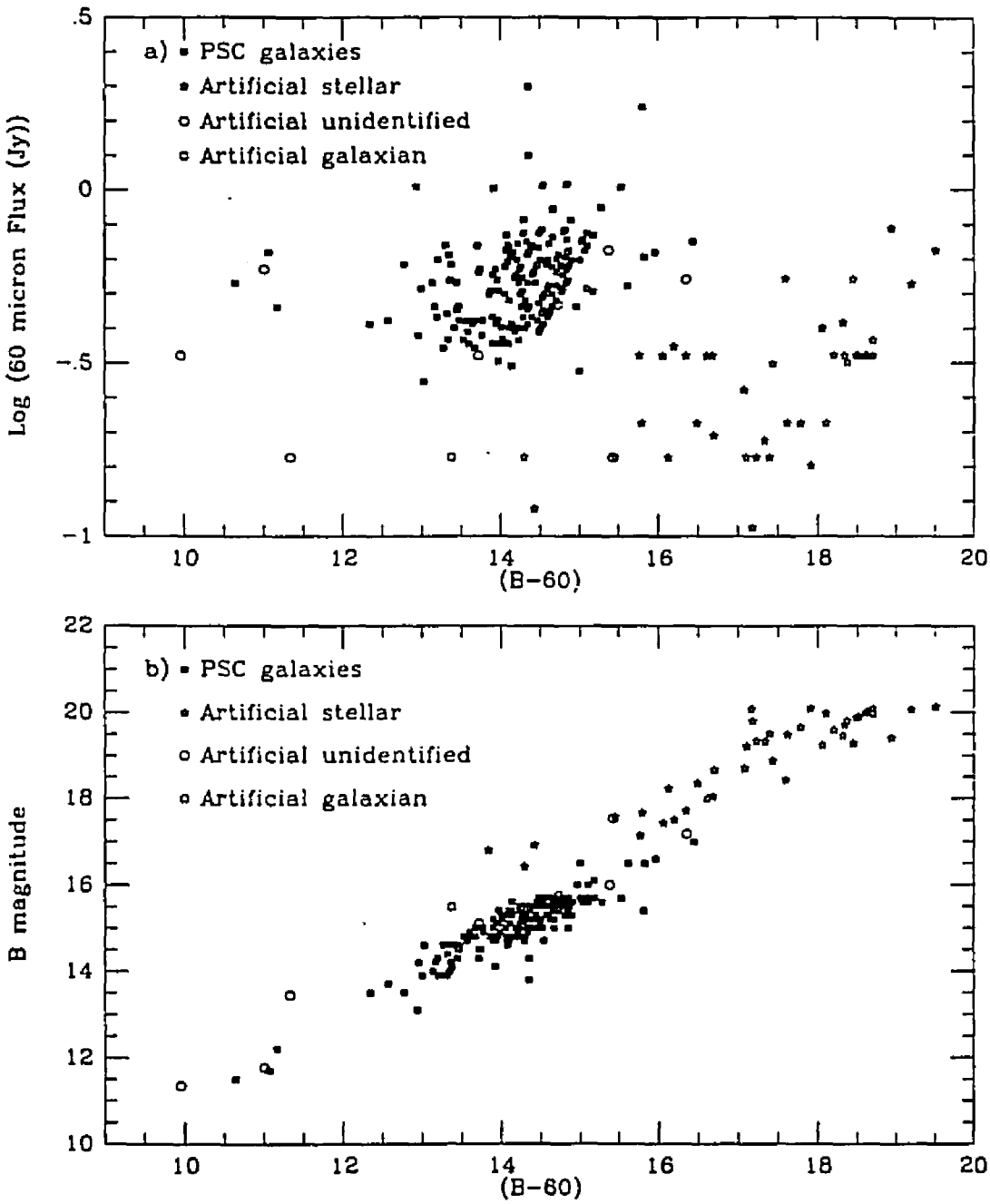

Figure 15. (B−60) color *vs.* a) log of the 60 μm flux (Jy) and b) blue magnitude for 204 galaxies from the PSC (plotted as closed squares) and 52 artificial (non-SSC) sources. Sources classified as stellar are plotted as open stars, those classified as galaxian are plotted as open squares, and unclassified sources are plotted as open circles. The plotted sources are those optical counterparts with the highest association probabilities.

in other catalogs. The associations of these 70 sources were compared to the PDS classifications to assess the level of agreement. Table 7 shows the breakdown of PSC associated galaxies, stars and quasars and the corresponding PDS classifications. The PDS classifications agreed with the PSC classifications best for PSC galaxies. For PSC stars, most of which were SAO stars (39 of 46), the PDS identifications were quite different. However, since the PDS classified by looking at the roundness of objects, the classification worked as expected by finding that many bright stars look non-round, due to their diffraction spikes. For PSC quasars, the PDS classified the optical sources as stellar. These data reflect the magnitude reliability range of the PDS scanning of POSS or ESO plates listed in Table 1: optical sources brighter than about 13 blue mag are not reliably classified.

B. Probability Histograms

Figure 16 contains histograms of the association probabilities of optical sources which have the highest association probability found around a) SSC 60 μm-only sources, b) SSC other sources and c) artificial sources. The fraction of sources with counterparts is binned by association probability, and the average probabilities for the three sets of data are stated. The association probabilities are higher for the

Table 7

COMPARISON OF CLASSIFICATIONS FROM THE IRAS PSC

70 Sources from the SSC and the PSC

PSC Classification	PDS Classification	Number Classified
Galaxy	g	13
	s	4
	a,x	2
	blank	3
Star	g	24
	s	5
	a,x	7
	blank	10
QSO	g	0
	s	2
	a,x	0
	blank	0

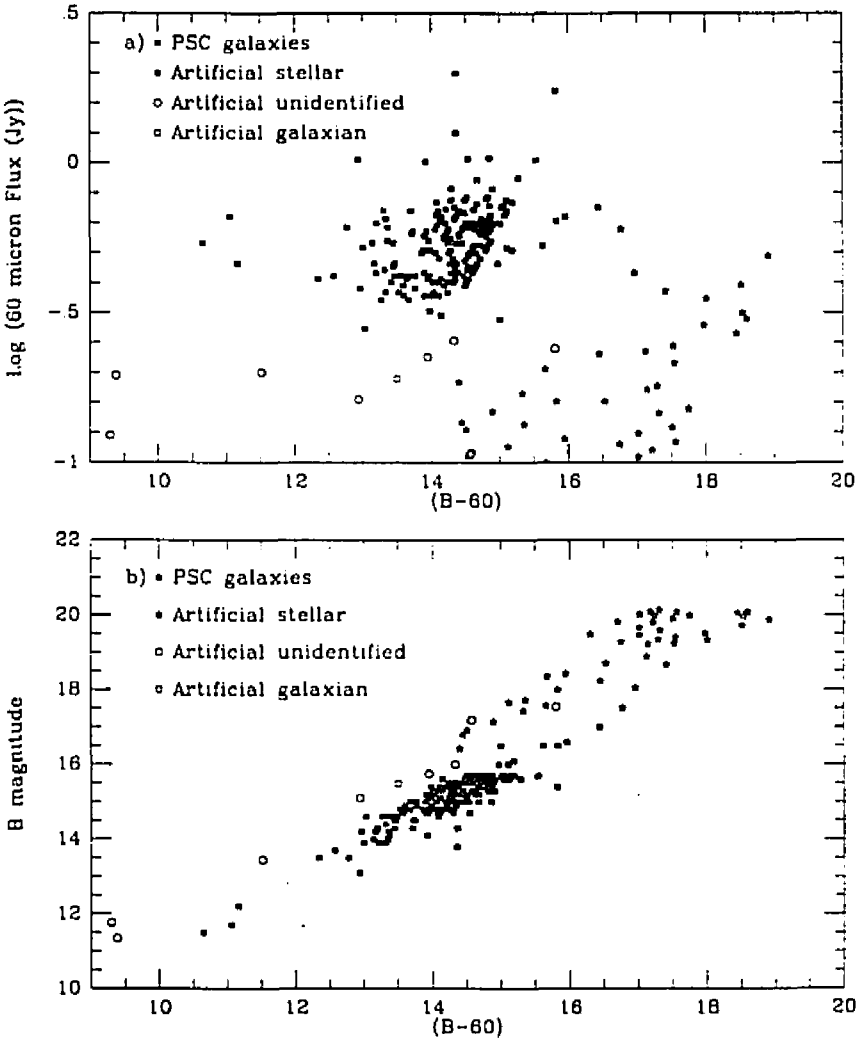

Figure 16. Probability histograms of optical counterpart candidates for a) SSC 60 μm-only sources, b) all other SSC sources and c) artificial data (randomly-placed sources). These histograms use the optical counterpart candidate with the highest association probability. They show that the probability of association is about the same for 60 μm-only and all other SSC sources, and that SSC sources have a higher probability of association than randomly placed artificial data.

SSC sources than for the artificial data, and are equal for 60 μm-only or all other sources. Note that association probabilities are lower for each optical counterpart candidate in an error box when there are more optical sources found. Since the average number of optical to IR sources is higher for the SSC data than for the artificial data, the association probabilities for the SSC data are actually better than reflected by the histograms. It is also important to note that 60 μm-only sources (under question here) have the same association probability as all other sources (whose reliability is not in question).

C. SSC Reliability Estimates

The majority of the 927 sources studied here have been found to have optical counterparts within their error boxes (89%). A test of random positions shows that less than 78% of the sources have optical counterparts. Whereas some of the SSC source blank fields may be explained by the presence of very bright objects which the PDS cannot 'see', the random positions contained no bright objects. Hence, the 89% is a lower limit of possible optical counterpart detections of SSC sources. It has also been shown that cirrus contamination is probably not a significant contributor to the surplus 60 μm sources. On average, there is one more optical counterpart candidate

to IR source for the SSC data than for the artificial data. Association probabilities of the SSC data are higher than those for the artificial data, as is the percentage of sources classified as galaxian or stellar. It appears that the overabundance of 60 μm-only sources have *bona fide* optical counterparts, and are thereby likely real astronomical objects.

D. Anomalies

Many of the 60 μm-only detections have been associated with faint spirals. Plots of the (B−60) colors indicate that the PDS found objects which it identified as galaxian which have colors similar to known spiral galaxies. The PDS also found many redder objects which it identified as stellar. These redder objects have colors more similar to those of quasars than to those of evolved stars. Both types of objects, spiral galaxies and quasars, typically have peak IRAS emission in the 60 μm band, so these findings agree with known characteristics of well-studied celestial objects. It appears that no new type of object has been found, but rather a fainter population of known ones has been cataloged.

The 99 blank fields found around the SSC sources may prove worthy of further study. There may exist optical counterparts beyond the completeness limits of

the AOs which are particularly interesting. Of the 99 PDS blank fields, 14 were SAO stars missed by the PDS, 45 were also deemed blank via visual inspection and 34 were labeled faint from the visual inspection. Figure 17 shows the flux distribution of the SSC sources around which the PDS detected no objects. Most of the blank sources have very low 60 μm fluxes and may likely have very faint optical counterparts.

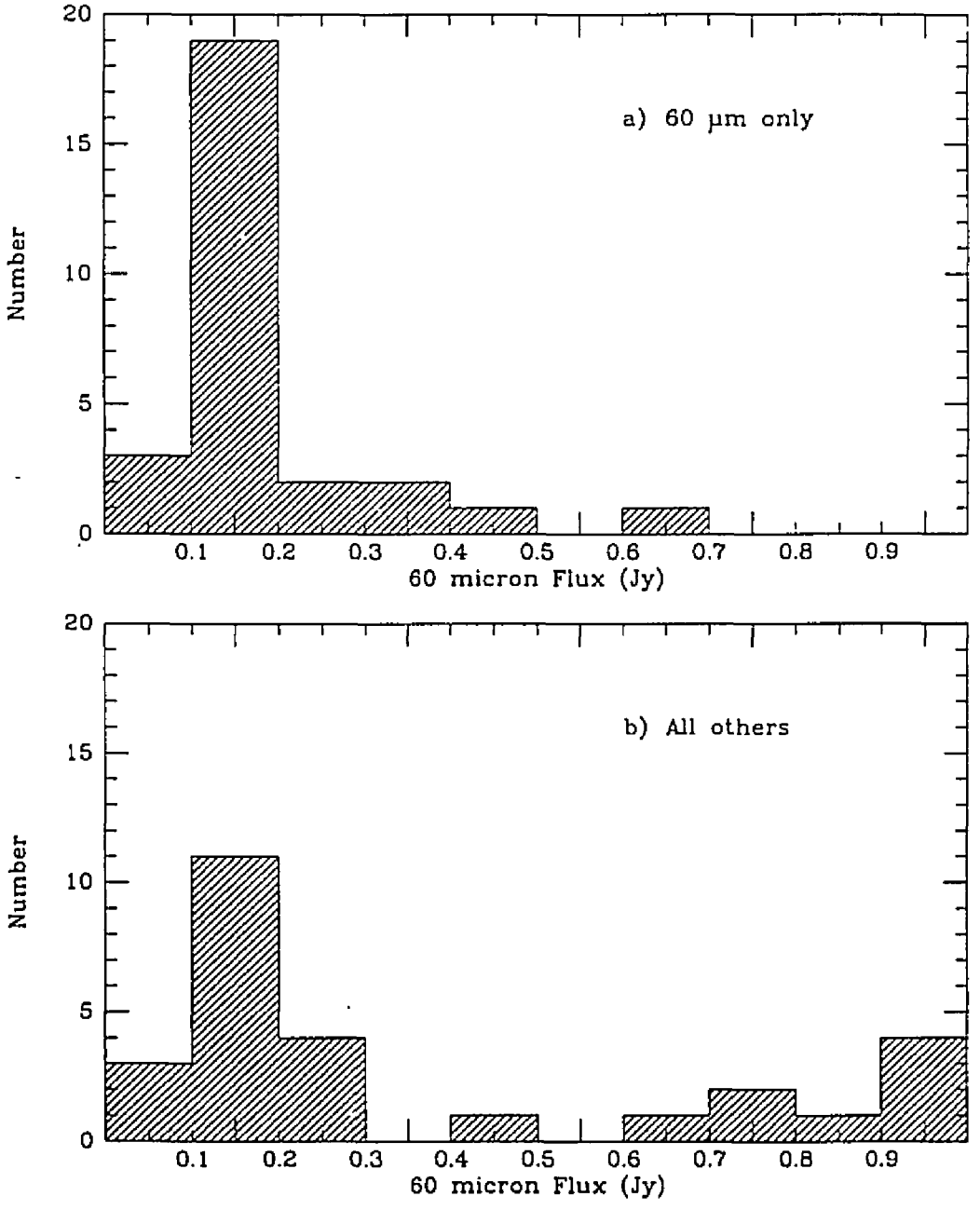

Figure 17. Histograms of the number of sources in a flux range of a) 60 μm-only and b) all other sources which appeared as blank fields to the PDS. SAO stars account for some of the bright other sources, but most of the 60 μm-only sources have low fluxes.

V. SUMMARY

A. Basic Question: Is The IRAS SSC Reliable?

The IRAS SSC catalogs a higher fraction of objects which emit only at 60 μm than has been previously cataloged in the PSC. This finding could be the result of an unusually low 60 μm sensitivity, or it could be an artifact of the process used to produce the catalog. Here, an optical counterpart identification program was initiated to try to determine the cause of the surplus of 60 μm-only objects. Cirrus was also studied to see what role it played in boosting the number of 60 μm detections in the SSC.

B. Method

A photographic plate-scanning program was conducted to try to identify optical sources associated with SSC sources. The AO fields with the highest densities of 60 μm detections at galactic latitudes $|b^{II}| \geq 30°$ were selected to be scanned. Since an average of 3.4 optical sources per IR source was found, a probability of association was estimated for each optical source. Using other PDS parameters, the optical sources were classified as galaxian, stellar or unidentifiable. Of 927 SSC sources

studied, 2778 optical counterpart candidates were found around 828 IR sources.

CCD photometry of the stars in four star clusters was performed by L. Davis (priv. comm.). POSS red and blue plates of these clusters were scanned with the NOAO PDS and the derived magnitudes were compared to the CCD values. Cross-calibrations between the CCD colors and the POSS/PDS colors were obtained. The data were fitted to third order polynomials with resulting 1σ uncertainties of 0.50 CCD mag for the blue data, and 0.41 CCD mag for the red. These calibrations were used to estimate blue magnitudes for the 2778 optical counterpart candidates.

The characterisitics of the optical counterparts to the SSC sources were compared to those of artificial data (with randomly chosen source positions). The artificial sources were further selected to represent 60 μm-only sources. This comparison showed that the characteristics of the SSC optical counterparts mimic those of well known celestial objects which are expected to have peak 60 μm emission. The artificial data was not so matched. On average, there were 2.1 optical sources per IR source for the artificial data, and 3.4 per source for the actual SSC sources. The SSC sources appear to have, on average, about one more optical source nearby than seen toward random positions.

The cirrus contamination across each AO field was studied from the Sky Flux images to assess the effect it might have on the overabundance of 60 μm-only sources. This analysis showed that cirrus did not appear to be correlated with the number of 60 μm detections in an AO.

The optical characteristics of the SSC 60μm-only sources were compared to the optical characteristics of the remainder of the SSC sources. This comparison showed that there are roughly equal probabilities of finding an optical counterpart for either type of source.

C. Results of the Study

None of the results presented here seem to indicate that the SSC contains spurious sources. In almost all cases (89%), the PDS identification method found optical counterpart candidates within the error bars of the SSC source positions. This is a lower limit because, in some cases, the visual inspection method showed that although the PDS reported a blank field, an object was seen adjacent to the SSC error box. This was especially true for brighter objects for which the PDS did not always find the true image center of the object (*e.g.*, SAO stars).

When the SSC sensitivity curve was made to imitate that of the PSC, there

were fewer 60 μm-only sources in the corrected sample (15 *vs.* 25%). (B−60) color plots of SSC objects classified as galaxian by the PDS show that such objects have colors most similar to faint spiral galaxies. These results imply that the extra 60 μm-only sources in the SSC are most likely due to the extra sensitivity in that band.

In comparison studies between 60 μm-only sources and all other sources in the sample, there were no large differences in the number of identified optical counterparts which could be associated with the IR sources. The results of the automated method used to classify PDS scanned objects as galaxian or stellar showed that 79% of the 60 μm-only and 75% of all other sources were classifiable. Although many of the most probably associated optical counterparts to the 60 μm-only sources were classified by the PDS as galaxian, many more of them were classified as stellar objects. Whereas many highly evolved stars will show blackbody spectra whose IRAS emission peaks at 25 or 60 μm, quasars are also stellar objects which have peak 60 μm IRAS emission. (B−60) color plots of PSC galaxies, SSC quasars, Carbon stars and S stars showed that the SSC objects classified by the PDS as stellar are more like quasars than evolved stars. Spectral classifications of these objects are necessary to confirm such identifications.

When the 60 μm-only and all other SSC data were compared to artificial data, the association probabilities were higher for the SSC data, and 60 μm-only sources had similar probabilities to all other sources; more of the SSC sources had optical counterparts (89 *vs.* 78%) than artificial sources; and there was, on average, one more optical counterpart candidate found in the search boxes around SSC sources than in the search boxes around artificial sources. These data imply that the 60 μm-only sources, which had similar statistics to all other SSC sources, are not likely spurious since they appeared to be significantly more reliable than randomly-placed artificial sources.

The conclusions drawn from this study indicate that there is no evidence to support the notion that the surplus of 60 μm-only sources in the SSC is due to spurious detections or to cirrus. The sources appear to be *bona fide* detections possessing characteristics similar to previously studied 60 μm peak emission objects.

The SSC is deemed reliable as probed by this study of 60 μm-only sources.

VI. REFERENCES

IRAS Sky Brightness Images. 1988, as described in the *IRAS Explanatory Supplement 1988.*

IRAS Catalog & Atlases: Explanatory Supplement 1988, ed. C. A. Beichman, G. Neugebauer, H. J. Habing, P. E. Clegg, and T. J. Chester (Washington, D. C.: U. S. Government Printing Office).

Christian, C. A., Adams, M., Barnes, J. V., Butcher, H., Hayes, D. S., Mould, J. R., and Siegel, M. 1985, *P. A. S. P.* **97**, 363.

Cutri, R.M., Clemens, C.M. and Low, F.J. 1987, *B. A. A. S.* **19**, 1066.

Huchra, J. P., Geller, M. J., Tokarz, S. P., Clemens, C. M., and Michel, A. 1991, **The CfA Redshift Catalog**, Springer Verlag, in press.

Huchra, J.P., *UV, Optical and IR Properties of Starforming Galaxies* in **Starbursts and Galaxy Evolution** Moriond Conf. 1987, TX Thuan, Th Montmerle and J. Tranh Than Van, Eds. (Paris: Editions Frontières) pp 199-214.

Kleinmann, S. G., Cutri, R. M., Young, E. T., Low, F. J., and Gillett, F. C. 1986, *Explanatory Supplement to the IRAS Serendipitous Survey Catalog* (Pasadena: JPL).

Stephenson, C. B. 1973, *A General Catalogue of Cool Carbon Stars* (*Pub. Warner and Swasey Obs.*, **1**, No. 4)

Stephenson, C. B. 1984, *A General Catalogue of S stars*, 2nd Ed., (Cleveland, Ohio: Case Western Reserve University)

Cataloged Galaxies and Quasars Observed in the IRAS Survey, Version 2 1989, prepared by C. J. Lonsdale, G. Helou, J. Good, and W. Rice (Pasadena: JPL).

Low, F.J. *et al.* 1984, *Ap. J. Lett.* **278**, L19.

Monet, D. G. 1983, **NASA Conf. Pub. 2317 on Astronomical Microdensitometry**, ed. D. A. Klinglesmith, 291.

Prestage, R.M. and Peacock, J.A. 1983, *M. N. R. A. S.* **204**, 355.

Rowan-Robinson, M., *et al.* 1984, *Ap. J. Lett.* **278**, L7.

Véron-Cetty, M. -P. and Véron, P. 1989, *A Catalogue of Quasars and Active Nuclei (4th Edition)* European Southern Observatory Scientific Report, Number 7.

Young, E. T., Neugebauer, G., Kopan, E. L., Benson, R. D., Conrow, T.P., Rice, W. L., and Gregorich, D. T. 1985, *A User's Guide to the IRAS Pointed Observation Products, IPAC preprint PRE-008N.*